

Middle Pleistocene genome calibrates a revised evolutionary history of extinct cave bears

Axel Barlow*^{1,2}, Johanna L. A. Paijmans³, Federica Alberti¹, Boris Gasparyan⁴, Guy Bar-Oz⁵, Ron Pinhasi⁶, Irina Foronova⁷, Andrey Y. Puzachenko⁸, Martina Pacher⁹, Love Dalén^{10,11}, Gennady Baryshnikov¹², Michael Hofreiter¹.

¹School of Science and Technology, Nottingham Trent University, Clifton Lane, Nottingham NG11 8NS, United Kingdom.

²Institute for Biochemistry and Biology, University of Potsdam, Karl-Liebknecht-Strasse 24–25, 14476 Potsdam, Germany.

³School of Archaeology and Ancient History, University of Leicester, University Road, Leicester LE1 7RH, UK.

⁴Institute of Archaeology and Ethnography, National Academy of Sciences of the Republic of Armenia, 0025, RA, Yerevan, 15 Charents st., Armenia.

⁵The Zinman Institute of Archaeology, University of Haifa, 199 Aba-Hushi Avenue, Haifa, Israel 3498838

⁶Department of Evolutionary Anthropology, University of Vienna, Althanstraße 14, 1090 Vienna, Austria.

⁷V.S. Sobolev Institute of Geology and Mineralogy, Siberian Branch of the Russian Academy of Sciences, 3, Ac. Koptuyuga ave., Novosibirsk, Russia, 630090.

⁸Institute of Geography, Russian Academy of Sciences, Staromonetnyy Pereulok, 29, Moscow, Russia, 119017.

⁹Institute of Paleontology, University of Vienna, Geozentrum, UZA II, Althanstraße 14, A - 1090 Vienna, Austria.

¹⁰Centre for Palaeogenetics, Stockholm University, SE-106 91 Stockholm, Sweden.

¹¹Department of Bioinformatics and Genetics, Swedish Museum of Natural History, Svante Ahrenius väg 3, 114 18 Stockholm, Sweden.

¹²Zoological Institute, Russian Academy of Sciences, Universitetskaya Naberezhnaya 1, 199034 St. Petersburg, Russia.

*Lead Contact: axel.barlow.ab@gmail.com

SUMMARY

Palaeogenomes provide the potential to study evolutionary processes in real time, but this potential is limited by our ability to recover genetic data over extended timescales [1]. As a consequence, most studies so far have focused on samples of Late Pleistocene or Holocene age, which covers only a small part of the history of many clades and species. Here, we report the recovery of a low coverage palaeogenome from the petrous bone of a ~360,000 year old cave bear from Kudaro 1 cave in the Caucasus Mountains. Analysis of this genome alongside those of several Late Pleistocene cave bears reveals widespread mito-nuclear discordance in this group. Using the time interval between Middle and Late Pleistocene cave bear genomes, we directly estimate ursid nuclear and mitochondrial substitution rates to calibrate their respective phylogenies. This reveals post-divergence mitochondrial transfer as the dominant factor explaining their mito-nuclear discordance. Interestingly, these transfer events were not accompanied by large-scale nuclear introgression. However, we do detect additional instances of nuclear admixture among other cave bear lineages,

47 and between cave bears and brown bears, which are not associated with mitochondrial exchange.
48 Genomic data obtained from the Middle Pleistocene cave bear petrous bone has thus facilitated a
49 revised evolutionary history of this extinct megafaunal group. Moreover, it suggests that petrous
50 bones may provide a means of extending both the magnitude and time depth of palaeogenome
51 retrieval over substantial portions of the evolutionary histories of many mammalian clades.
52

53 **KEYWORDS**

54 Palaeogenomics, ancient DNA, cave bear, *Ursus*, Middle Pleistocene, evolution
55

56

57 **RESULTS AND DISCUSSION**

58 Analyses of palaeogenomes have provided unparalleled insights into the evolution of numerous
59 vertebrate lineages. Assembling these datasets represents a considerable technical challenge,
60 however, due to postmortem degradation and the loss of endogenous DNA molecules over time [1].
61 This is especially true for warm temperate and tropical environments, where DNA degradation
62 proceeds more rapidly than in colder boreal or arctic environments [1]. As a consequence,
63 comparatively few ancient DNA studies have successfully retrieved genetic data from temperate
64 zone samples of Middle Pleistocene age (Chibanian age, 129–774 ka [2]). Notable successes
65 include high coverage genome datasets from samples dating around the Middle to Late Pleistocene
66 boundary from Germany [3,4] and from the Altai Mountains [5]. Much older DNA sequences have
67 been retrieved from samples dating to ~430 ka from Spain, but with a lower magnitude of data
68 recovery, comprising of mitochondrial genome sequences [6,7] and 1–2 megabases of nuclear DNA
69 [8]. Nonetheless, these achievements suggest that the retrieval of genome-scale datasets of this age
70 is possible, provided samples of sufficient quality can be found.
71

71

72

73 ***Middle Pleistocene cave bear genome***

74 One recent and notable advance in palaeogenome sequencing has been the discovery of the
75 mammalian petrous bone as a source of high purity ancient DNA [9]. One group where this
76 approach has been successfully applied are extinct cave bears [10,11], which form the sister lineage
77 to the clade consisting of the extant brown (*Ursus arctos*) and polar (*Ursus maritimus*) bears. To
78 investigate if petrous bones may provide a way of extending both time depth and magnitude of
79 Middle Pleistocene genome data retrieval, we investigated the petrous bone of a Middle Pleistocene
80 cave bear from Kudaro 1 cave located in South Ossetia in the Southern Caucasus. The sedimentary
81 layer (5c) from which this sample was recovered has been dated using radiothermoluminescence at
82 $360,000 \pm 90,000$ years [12], and multiple additional sources of evidence support a Middle
83 Pleistocene age for the specimen (see STAR Methods). The Kudaro 1 sample is assigned to the
84 taxon *Ursus kudarensis praekudarensis*, which is thought to be ancestral to the Late Pleistocene
85 Caucasian cave bear *U. k. kudarensis* based on morphological evidence [13,14].
86

86

87 We extracted DNA from the *praekudarensis* petrous bone and sequenced it using Illumina
88 technology. From a total of ~2.6 billion sequenced molecules, we were able to map 2.1 Gb of
89 sequence with high confidence to the reference genome assembly of the polar bear (Table S1). This
90 represents a low coverage genome dataset where the majority of sequenced positions are covered by
91 a single sequencing read (Figure S1). The estimated proportion of endogenous DNA molecules in
92 the *praekudarensis* extract is 3.6% (Table S1), which is remarkable given the age of the specimen,

93 and exceeds the endogenous proportions of some previously studied temperate-zone Middle
94 Pleistocene extracts [8] by several orders of magnitude.

95
96

97 ***Cave bear nuclear and mitochondrial relationships are highly incongruent***

98 Phylogenetic relationships among cave bear taxa have been largely guided by analysis of their
99 mitochondrial DNA [15,16]. Our previous study on nuclear genomes did reveal one instance of
100 mito-nuclear discordance among three Late Pleistocene taxa [10], but the limited sampling of this
101 study precluded a broader assessment of cave bear nuclear relationships. To investigate this further,
102 we analysed the Middle Pleistocene *praekudarensis* genome dataset alongside novel genome
103 datasets of Late Pleistocene cave bears generated from their petrous bones, representing the taxa
104 *rossicus* (Kizel Cave, Ural Mountains, Russia), *kanivetz* (Medvezhiya Cave, Ural Mountains,
105 Russia), and *kudarensis* (Hovk 1 Cave, Armenia). We also included published datasets from the taxa
106 *spelaeus* (Eiros Cave, Spain) [10], *eremus* (Windischkopf Cave, Austria) [10], *ingressus*
107 (Gamssulzen Cave, Austria) [11], and a second *kudarensis* individual from Hovk 1 Cave [10] in
108 addition to modern Georgian and Late Pleistocene Austrian brown bears [10], two modern polar
109 bears [17], and a modern Asiatic black bear [18] as outgroup (see Table S1 & S2).

110

111 We investigated relationships among the cave bear nuclear genomes using Principal Components
112 Analysis (PCA). This involved sampling a single mapped nucleotide from each individual at each
113 position of the reference genome, which provided data from a total of 487,747 variable transversion
114 sites after strict filtering (STAR Methods). PCA suggested three major groups (Figure 1A)
115 comprising: the Caucasus cave bears *praekudarensis* and *kudarensis*, which cluster together as
116 predicted by morphology; a second, geographically widespread and broadly European group
117 including *spelaeus*, *ingressus*, *eremus*, and *kanivetz* from the Urals; and finally, the Urals cave bear
118 *rossicus*, which is distinct from all other cave bears and may represent a Urals-specific group. PCA
119 further suggests a hierarchy of relationships within these groups, with each successive PC
120 separating different taxa from one another (Figure 1B).

121

122 The three major groups identified by the PCA deviate from expectations based on mitochondrial
123 DNA, which instead supports two major clades comprising the Caucasus cave bears and all
124 European and Urals cave bears, respectively, with *rossicus* nested within the latter (Figure 1C). We
125 further investigated these contrasting nuclear relationships using phylogenetic analysis, including
126 representative brown bears, polar bears and the Asiatic black bear outgroup. Palaeogenomic datasets
127 are generally associated with high rates of error, which can distort estimates of phylogenetic branch
128 lengths when only a single read is sampled [11]. We therefore applied a recently developed method,
129 Consensify [11], which calls the majority base from a random sample of three mapped nucleotides.
130 This method provided a single high quality allele from each individual for a total of 4,318,414
131 genomic sites, of which 39,122 were variable. Maximum likelihood phylogenetic analysis of this
132 dataset (Figure 1D) supported the expected relationships between polar bears, brown bears, and the
133 cave bear clade, as well as the position of the Caucasus cave bears within the latter. Among the
134 sampled cave bears from Europe and the Urals, however, there is not a single sister-group
135 relationship that agrees between the mitochondrial and nuclear phylogenies.

136

137 The relationships among cave bears inferred using nuclear DNA closely match estimates based on
138 morphological characters [19,20], in contrast to mitochondrial relationships, which are frequently

139 incongruent with morphology. Mitochondrial DNA, which has provided the basis for our
140 understanding of cave bear relationships for several decades, thus emerges as a phylogenetic outlier
141 in contradiction with generally congruent evidence from morphology and nuclear genomes.
142 Mitochondrial evolution in cave bears therefore appears to have been shaped to a large extent by
143 incomplete lineage sorting and/or gene flow among cave bear lineages, as previously documented in
144 brown bears and polar bears [17].

145
146 The revised cave bear nuclear genome phylogeny provides several new insights into their evolution.
147 Consistent with the results of the nuclear PCA, the Uralian cave bear *rossicus* represents a deeply
148 divergent and isolated phylogenetic lineage (Figure 1D), supporting its recognition as a third major
149 cave bear group, which has been obscured until now due to reliance on mitochondrial DNA. Within
150 the European cave bear group, three large bodied taxa, *spelaeus*, *ingressus* and *kanivetz*, form a
151 clade that is sister to the smaller bodied cave bear *eremus*. This suggests a single increase in body
152 size in their common ancestor, rather than two independent shifts as previously inferred from their
153 mitochondrial relationships [15]. Moreover, the validity of the taxon *kanivetz* has itself been
154 questioned by mitochondrial phylogeographic studies [15], which show it to be nested within the
155 wider *ingressus* mitochondrial clade. Nuclear genome analysis, however, supports its
156 distinctiveness and position as sister to the European taxa *spelaeus* and *ingressus*. Finally, the first
157 three primary phylogenetic divisions of cave bears involve Uralian or Asian lineages, potentially
158 reflecting an eastern origin for what has traditionally been regarded as a European radiation [21].

159 ***Direct estimation of the genome-wide substitution rate***

161 The temporal gap between *praekudarensis* and its Late Pleistocene sister lineage *kudarensis*
162 provides an opportunity to estimate the *Ursus* substitution rate and calibrate the revised nuclear
163 phylogeny of cave bears. We calculated the difference in their respective genetic divergences to
164 modern brown bear and polar bear outgroups using the 4,318,414 Consensify error-reduced nuclear
165 positions, which provides an estimate of the number of nucleotide substitutions occurring during
166 their sampling interval. Based on the median *praekudarensis* radiothermoluminescence date and the
167 age estimates of the *kudarensis* samples (Table S2), this equates to 305,400 years and yields a
168 genome-wide nuclear substitution rate of 9.56×10^{-10} substitutions/site/year (range $7.39\text{--}13.56 \times 10^{-10}$
169 10 substitutions/site/year accommodating the radiothermoluminescence date uncertainty, Table S3).
170 This estimate is substantially slower than ancient-DNA derived estimates for dogs and wolves
171 ($\sim 1.2 \times 10^{-8}$ [22]), but exceeds published estimates for humans and other great apes [23]. Notably,
172 our estimated *Ursus* substitution rate is approximately double that estimated for humans (5×10^{-10}
173 substitutions/site/year [24]), which aligns well with the difference in their respective generation
174 times (brown and polar bears 11–12 years [25,26], humans 20–25 years [27,28]), suggesting their
175 underlying per-generation nuclear mutation rate is approximately equal. Applying the same
176 methodology to mitochondrial DNA (excluding the control region) produced an estimated *Ursus*
177 mitochondrial substitution rate of 1.81×10^{-8} substitutions/site/year (range $1.40\text{--}2.57 \times 10^{-8}$
178 substitutions/site/year, Table S3). This estimate falls within the lower range of mitochondrial
179 substitution rate estimates for other vertebrates [29]. It also overlaps with estimated rates for human
180 mitochondrial DNA [30], deviating from the ratio predicted by generation times and suggesting
181 some difference in the underlying rate of mitochondrial mutations between humans and bears.

182
183 We used these newly estimated substitution rates to calculate absolute times of nuclear and
184 mitochondrial divergence for all pairs of individuals (Figure 2, Tables S4 and S5), and calibrate

185 their respective phylogenies (Figure 3). We note that the divergence times of genetic lineages will
186 be older than the divergence of their respective populations as they likely include standing variation
187 in the ancestral population. However, since the lineages under study span a large evolutionary
188 timescale and show high levels of structuring (see D-statistic analysis below), the obtained times
189 most likely provide reasonable approximations. Median nuclear divergence time estimates of cave
190 bears and their sister clade, polar bears and brown bears, were found to be around 1.52 Ma (Figures
191 2A and 3). The mitochondrial divergence time is similar, around 1.48 Ma (Figures 2A and 3). These
192 estimates are more recent than most previous estimates based on mitochondrial DNA, but highly
193 consistent with the fossil record (see STAR Methods). Median estimates for the polar bear and
194 brown bear nuclear divergence are around 0.99 Ma (Figures 2B and 3), which is highly similar to
195 previous phylogenetic estimates [18]. Median nuclear divergence times of the three major cave bear
196 clades also fall around the same time, around 0.98 (Figures 2C and 3) and 0.87 Ma (Figures 2D and
197 3). Notably, these primary divergence events among cave bears, as well as between brown bears and
198 polar bears, coincide with the Middle Pleistocene Transition, 1.2–0.8 Ma, when glacial cycles
199 shifted from a ~40 to a ~100 ka periodicity causing extended glacial periods and more abrupt,
200 intense interglacials [31], which may have been a factor promoting their divergence. Within the
201 Caucasian cave bears, we find a comparatively deep divergence time between *kudarensis* and
202 *praekudarensis* (median estimate ~495 ka at the age of *praekudarensis*; Figures 2E and 3),
203 potentially arguing against the direct ancestor descendant-relationship suggested by morphology, or,
204 alternatively, for a genetically structured *praekudarensis* population. Among the European cave
205 bears, we find a comparatively rapid sequence of divergence events among the four sampled taxa
206 (median ages 427–344 ka, Figures 2F and 3), which are notably older than previous estimates based
207 on mitochondrial DNA [15,32].

208
209

210 ***Mitochondrial transfer explains mito-nuclear discordance in cave bears***

211 Time calibration of the nuclear and mitochondrial cave bear phylogenies could reveal the
212 underlying causes of their discordance. Specifically, mitochondrial coalescence that considerably
213 post-dates the respective nuclear coalescence of taxa implies the transfer of mitochondrial DNA
214 through admixture. Examination of cave bear pairs exhibiting mito-nuclear discordance (defined as
215 pairs with different taxa descending from the ancestral nodes of their respective nuclear and
216 mitochondrial clades) reveals that all pairs but one (*spelaeus* and *ingressus*) show mitochondrial
217 coalescence that is more recent than their respective nuclear coalescence (Figure 2, Tables S3 and
218 S4), implicating mitochondrial transfer as the dominant factor shaping their mitochondrial
219 relationships.

220

221 Multiple alternative transfer scenarios could explain the observed mitochondrial relationships, and
222 selecting among them is challenging based on the available data. One notable set of comparisons
223 are those involving the Uralian cave bear *rossicus* and the European cave bears *ingressus* and
224 *kanivetz*, whose mitochondrial coalescence times post-date their respective nuclear coalescence by
225 more than 700 ka (Figure 2D). Since none of the sampled European or Uralian mitochondrial
226 lineage pairs approaches the nuclear coalescence of *rossicus* and the European cave bear group
227 (median estimate ~0.87 Ma), it seems most likely that *ingressus* or *kanivetz* transferred its
228 mitochondrial DNA to *rossicus*, although alternative scenarios such as multiple transfers or back
229 transfers cannot be conclusively excluded. Also notable are mitochondrial coalescence times of the
230 European cave bears *spelaeus* and *eremus*, and *ingressus* and *kanivetz*, which both considerably

231 post-date their respective nuclear divergences (> 290 ka based on median substitution rate
232 estimates; Figure 2F), implicating mitochondrial transfer also between lineages of these pairs.
233 Determining the direction of these transfer events is challenging due to the rapid sequence of
234 nuclear divergence events in European cave bears, around which many of their mitochondrial
235 coalescence events also cluster (Figure 2F). The precise history of mitochondrial evolution is likely
236 to remain uncertain until genetic data from samples pre-dating the inferred mitochondrial transfer
237 events is obtained, which would require obtaining DNA sequences from multiple additional Middle
238 Pleistocene specimens.

239

240

241 ***Mitochondrial transfer is not strongly associated with nuclear introgression***

242 Since our analyses reveal numerous instances of mitochondrial transfer among cave bears, we
243 investigated evidence of nuclear gene flow using D-statistic analysis of the error reduced genome
244 sequences, which has been shown to represent a conservative approach that is more resistant to false
245 positives than other methods [11]. Interestingly, we failed to detect nuclear gene flow among those
246 cave bear taxa implicated in mitochondrial transfer events (Figure 4), suggesting that any residual
247 nuclear introgression resulting from these gene flow events is below the detection threshold of our
248 low coverage genome datasets. In fact, only a single nuclear gene flow event is detected among the
249 sampled cave bear lineages, between the lineage leading to *kudarensis* and the lineage leading to the
250 European cave bears (Figure 4). Notably, this nuclear admixture event is not accompanied by any
251 evidence of mitochondrial transfer. Similarly, we have previously shown that gene flow occurred
252 between cave bears and brown bears [10], again with no evidence of mitochondrial exchange.
253 Replicating these tests including our novel cave bear genomes consistently supports this previous
254 result, and moreover, our improved sampling pinpoints the common ancestor of the European and
255 Uralian cave bears as the admixing cave bear lineage (Figure 4), with no evidence of gene flow
256 following the divergence of its descendant clades.

257

258 This disparity between instances of nuclear and mitochondrial introgression within a recently
259 diverging clade is puzzling. Enhanced mitochondrial introgression is documented in species with
260 male-biased dispersal, such as bears, since this reduces the effective population size of maternally
261 inherited loci in the incoming species at the contact zone [33]. However, this process does not
262 explain the apparent absence of mitochondrial mixing among Caucasian and European cave bears,
263 or among cave bears and brown bears. Here, some additional factor, such as a complete absence of
264 females representing the incoming species, preferential mating of hybrids with their maternal
265 species, or asymmetrical hybrid sterility [34], must have operated.

266

267

268 ***Conclusions***

269 We have shown that petrous bones provide a way to extend both the time depth and magnitude of
270 Middle Pleistocene genome sequencing. The palaeogenome of the Middle Pleistocene
271 *praekudarensis* cave bear sequenced in this study has provided important insights into the evolution
272 of this iconic group of extinct animals. Critically, by providing a means of calculating the genome
273 substitution rate, it has calibrated their evolutionary history, revealed numerous instances of
274 mitochondrial transfer, and suggested a potential link between a profound change in climate
275 dynamics and the divergence of major evolutionary lineages.

276

277 Palaeogenomes provide the opportunity to study the process of evolution in real time. For many
278 temperate zone species, however, the current time depth for palaeogenome recovery represents a
279 comparatively small part of their total evolutionary history. The age of the *praekudarensis* genome
280 pre-dates the origin of some cave bear taxa and encompasses an estimated 24% of the total
281 evolutionary history of cave bears. Petrous bones may thus thus provide a means of extending the
282 time depth of palaeogenome recovery over substantial fractions of the evolutionary histories of
283 many temperate zone species.

284

285

286 **AUTHOR CONTRIBUTIONS**

287 In alphabetical order: Conceptualization AB, GB, MH; Data curation AB; Formal analysis AB,
288 JLAP; Funding acquisition MH; Investigation FA, MP; Methodology AB; Project administration
289 AB, LD, MH; Resources BG, EB, GB, GB-O, IF, LD, RP; Software AB, JLAP; Supervision AB,
290 AP, GB, MH; Validation AB, JLAP; Visualization AB; Writing – original draft AB; Writing –
291 review & editing all authors.

292

293

294 **ACKNOWLEDGMENTS**

295 We pay tribute to our coauthor Irina Foronova for her contributions to the field of palaeontology,
296 who sadly passed away prior to the publication of this study. We thank Anthony J. Stuart for his
297 help collecting radiocarbon dates of Ural cave bears. The authors would like to acknowledge
298 support from the Science for Life Laboratory, the National Genomics Infrastructure (NGI), Sweden,
299 the Knut and Alice Wallenberg Foundation and UPPMAX for providing assistance in massively
300 parallel DNA sequencing and computational infrastructure. This work was funded by European
301 Research Council (ERC) consolidator grant ‘gene flow’ 310763 to M.H. The study was fulfilled
302 within a framework of the Federal theme of the Theriology laboratory of Zoological Institute of the
303 Russian Academy of Sciences no. AAAA-A19-119032590102-7 "Phylogeny, morphology and
304 systematics of placental mammals" and project "The evolution of the organic world. Role and
305 influence of planetary processes (subprogram I. Development of life and biosphere processes)" and
306 Program of the Russian Academy of Sciences Presidium and the Russian Ministry of Education and
307 Science "Evolution of the organic world. The role and significance of planetary processes" (2019)
308 (GB), and the Federal theme of the Laboratory of Biogeography of Institute of Geography of the
309 RAS no. AAAA-A19-119021990093-8 "Evaluation of physical and geographical, hydrological, and
310 biotic environmental changes and their effects for the base of sustainable environmental
311 management" (AP) and supported partly by a RFBR grant to AP (17-01-00100-a); and on the state
312 assignment of V.S. Sobolev Institute of Geology and Mineralogy, Siberian Branch of the RAS (IF).

313

314

315 **DECLARATION OF INTERESTS**

316 The authors declare no competing interests.

317 **MAIN TEXT FIGURE TITLES AND LEGENDS**

318

319 **Figure 1. Cave bear relationships.**

320 A. Ordination of individual cave bears along the first and second principal components of a PCA
321 based on 487,747 filtered transversion sites supports three major groups.

322 B. Ordination of the same individuals along PC3–PC6, which separate, respectively: *eremus*,
323 *kanivetz*, *kudarensis* and *praekudarensis*, and *ingressus* and *spelaeus*

324 C. Mitochondrial phylogeny based on 16,383 bp of aligned sequence and rooted using the Asiatic
325 black bear outgroup (not shown). Bootstrap support is 100% for all nodes.

326 D. Nuclear phylogeny based on 39,122 filtered, error-reduced variable sites. Rooting and bootstrap
327 support are as described for C. There are multiple instances of mito-nuclear discordance within the
328 European cave bears, among the European and Uralian cave bears, and among brown bears and
329 polar bears.

330

331 **Figure 2. Pairwise nuclear and mitochondrial divergence times.**

332 Points indicate ages estimated from substitution rates calculated using the median
333 radiothermoluminescence age of the *praekudarensis* sample of 360 ka. Error bars represent the
334 maximum and minimum ages reflecting the ± 90 ka uncertainty of the radiothermoluminescence
335 age (See Tables S3–S5). Note that since the age uncertainties of the pairwise estimates are not
336 independent, the rank order and relative separation of the point estimates will be maintained
337 irrespective of the true *praekudarensis* age. Sample pairs showing mito-nuclear discordance are
338 marked with asterisks. Results for specific clades discussed in the text are indicated (A–F).

339

340 **Figure 3. Calibrated nuclear and mitochondrial phylogenies.**

341 Branches terminate at the sample ages and nodes are centered on the mean of their respective
342 pairwise estimates (See Figure 2 and Tables S3–S5). The complete mitochondrial evolutionary
343 history of the European and Uralian cave bears is uncertain. The three recent mitochondrial transfer
344 events that can be inferred from pairwise estimates (Figure 2) are indicated by vertical arrows.
345 Shaded trapezoids connecting lineages indicate the two major episodes of nuclear gene flow
346 identified by D-statistic analysis, and are coloured consistently with Figure 4.

347

348 **Figure 4. D-statistics tests of cave bear admixture.**

349 Results are expressed as $D(P1,P2,P3,P4)$ with significant positive values (filled circles) indicating
350 admixture between P2 and P3 subsequent to the divergence of P1 and P2, coloured consistently
351 with the shaded trapezoids in Figure 3. To aid visualisation, the assignment of the P1 and P2
352 individuals has been adjusted to make their respective D value positive. The results indicate two
353 major episodes of nuclear gene flow among the sampled lineages: between brown bears and the
354 ancestor of the European and Uralian cave bears, subsequent to their divergence from their
355 respective sister lineages, polar bears $D(\text{polar,brown,cave,out})$ and the Caucasian cave bears
356 $D(\text{Caucasian,European/Uralian,brown-polar,out})$; and between *kudarensis* and the ancestor of the
357 European cave bears subsequent to their divergence from their respective sister lineages,
358 *praekudarensis* $D(\text{praekudarensis,kudarensis,European/Uralian,out})$ and the Uralian cave bear
359 *rossicus* $D(\text{Uralian,European,Caucasian,out})$.

360 **STAR METHODS**

361

362 **RESOURCE AVAILABILITY**

363

364 *Lead contact*

365 Further information and requests for resources should be directed to and will be fulfilled by the
366 Lead Contact, Axel Barlow (axel.barlow.ab@gmail.com).

367

368 *Materials availability*

369 This study did not generate new unique reagents.

370

371 *Data and code availability*

372 The raw, unprocessed sequencing reads in fastq file format, in addition to the processed data
373 mapped to each reference genome in bam file format, are available at the European Nucleotide
374 Archive (ENA), accessions [submitted awaiting accessions]. Novel cave bear consensus
375 mitochondrial sequences are available at the NCBI nucleotide database, accessions [submitted
376 awaiting accessions].

377

378 **EXPERIMENTAL MODEL AND SUBJECT DETAILS**

379 The novel cave bear datasets generated for this study are: *praekudarensis* (KU1), *kudarensis*
380 (HV72), *rossicus* (B05), and *kanivetz* (B04). These were generated from subfossil petrous bone
381 samples. Details of sample localities and ages are shown in Table S2.

382

383 Several sources of evidence support a Middle Pleistocene age of layer 5c in Kudaro 1 Cave, from
384 which the *praekudarensis* petrous bone was recovered: layer 5c has been dated using
385 radiothermoluminescence at $360,000 \pm 90,000$ yBp, and the overlying layer 5b has been dated
386 using the same method at $350,000 \pm 70,000$ yBp [12,35,36]; geomorphological studies of river
387 terraces of the Caucasus [37] suggest the cave entrance of Kudaro 1 was opened 300–400 thousand
388 years ago; archaeological material recovered from layer 5c belongs to the later Acheulean [36]; and
389 other faunal material recovered from layer 5c is consistent with a Middle Pleistocene age [38],
390 including *Macaca sp.*, *Canis mosbachensis*, *Panthera gombaszoegensis* and *Stephanorhinus*
391 *hundsheimensis* (the rhinoceros was identified by [39] as *Dicerorhinus etruscus brachycephalus*).
392 According to European markers, this faunal composition would suggest an even older age than
393 indicated by the radiothermoluminescence dates. However, the Caucasus region is considered to
394 represent a refugial area during the Pleistocene, which may explain the apparently more recent
395 occurrence of these taxa in Kudaro 1 compared to Middle Pleistocene European deposits.

396

397 The *rossicus* and *kanivetz* samples have not been directly dated. For the purpose of molecular dating
398 analyses, we used an indirectly estimated age for these samples based on the median age of
399 radiocarbon dated cave bear bones from these sites (Table S6).

400

401

402 **METHOD DETAILS**

403

404 *Laboratory methods*

405 Six sequencing libraries (KU1_1–KU1_6) were prepared from the *praekudarensis* KU1 sample for
406 this study. For the *kudarensis* sample HV72 we had previously prepared seven sequencing libraries
407 (HV72_1–HV72_7) and carried out low level sequencing. Six of these libraries (HV72_2 –
408 HV72_7) are described in [40]. We prepared one additional library (HV72_8) from this sample for
409 this study, which was used for deeper sequencing. Single libraries were prepared from the *rossicus*
410 B05 and *kanivetz* B04 samples.

411

412 For each library, bone was sampled from the otic capsule of the cave bear petrous bones [41] and
413 ground to a fine powder using a RETSCH mixer mill mm 400 at a frequency of 30 Hz for 10
414 seconds. DNA was then extracted using a published protocol optimized for the recovery of short
415 ancient DNA fragments [6], with the modifications described in [42]. 50 mg of bone powder was
416 digested in 1 mL of extraction buffer (0.45 M EDTA, 0.25 mg/mL Proteinase K) overnight at 37°C,
417 with rotation. Centrifugation was used to pellet any undigested material. The supernatant was
418 removed, combined with 13 mL of binding buffer (5 M guanidine hydrochloride, 40% (vol/vol)
419 isopropanol, 0.05% Tween-20, and 90 mM sodium acetate), and then passed through a commercial
420 silica spin column (Qiagen MinElute) fitted with an extension reservoir (Zymo- spin V). Two wash
421 steps were then carried out using PE buffer (Qiagen). Purified DNA was then eluted in two steps
422 each using 12.5 µL TET buffer (10mM Tris-HCl, 1 mM EDTA, 0.05% Tween-20).

423

424 Illumina sequencing libraries were prepared from the DNA extracts using a published protocol
425 based on single stranded DNA, optimised for the recovery of short ancient DNA fragments [43],
426 with the modifications described in [42]. DNA was treated with the enzymes uracil-DNA
427 glycosylase and Endonuclease VIII, to excise uracils resulting from the deamination of cytosine
428 residues and to cleave DNA strands at abasic sites, in 44 µL reactions with the following reagent
429 concentrations: 1.8x CircLigase buffer II, 4.5 mM MnCl₂, 0.11 U/µL of uracil-DNA glycosylase,
430 and 0.02 U/µL of endonuclease VIII. Residual phosphate groups were then removed from the
431 template DNA fragment ends using 1 unit of FastAP. The DNA was then heat denatured, and oligo
432 CL78 ligated to the 3' single-stranded fragments ends during overnight incubation in 80 µL
433 reactions with the following reagent concentrations: 20% (vol/vol) PEG-4000, 0.125 mM CL78,
434 and 2.5 units/µL CircLigase II. Ligation products were then immobilised on streptavidin beads
435 (MyOne C1) to allow the removal of reagent mixtures in subsequent library preparation steps. The
436 CL9 extension primer was annealed to the complementary CL78 oligo sequence and the strand
437 complementary to the template single-stranded molecules filled-in using Bst 2.0 polymerase in 50
438 µL reactions with the following reagent concentrations: 1x isothermal amplification buffer, 250 mM
439 of each dNTP, 2 mM CL9 extension primer, and 0.48 U/µL Bst 2.0 polymerase. T4 DNA
440 polymerase was then used to remove 3' overhangs, in 100 µL reactions with the following reagent
441 concentrations: 1x Buffer Tango, 0.025% (vol/vol) Tween 20, 100 mM of each dNTP, and 0.05
442 U/µL T4 DNA polymerase. The double-stranded adaptor (CL53/CL73) was then ligated to the
443 blunt-ended molecules using T4 DNA ligase in 100 µL reactions with the following reagent
444 concentrations: 1x T4 DNA ligase buffer, 5% (vol/vol) PEG-4000, 0.025% (vol/vol) Tween 20, 100
445 mM double-stranded adaptor, and 0.1 U/µL T4 DNA ligase. The library strand complementary to
446 the original single-stranded template molecule was then heat denatured and eluted in 25 µL TET
447 buffer.

448

449 Template library molecules were PCR amplified using AccuPrime Pfx polymerase, incorporating
450 unique 8 base-pair (bp) index sequences within both P5 and P7 adapters, in 80 µL reactions with the

451 following reagent concentrations: 1x AccuPrime Pfx reaction mix, 0.4 mM each of P5 and P7
452 indexing primers, and 0.025U/ μ L AccuPrime Pfx polymerase. Prior to library amplification, qPCR
453 analysis of the unamplified library was used to identify the appropriate number of PCR cycles,
454 corresponding to the cycle number at the point of inflection of the qPCR amplification curve,
455 corrected for differing reaction volume and template amount in the subsequent library amplification
456 PCR. The qPCR analysis involved 10 μ L reactions with the following reagent concentrations: 1x
457 SYBR green qPCR master mix, 0.2mM each of IS7 and IS8 amplification primers, and 0.2% of the
458 unamplified library. After amplification, the indexed libraries were quantified using a TapeStation
459 2200 instrument (Agilent) with D1000 screen tape and reagents, and a Qubit 2.0 instrument (Fisher)
460 with the dsDNA HS Assay kit. Sequencing of the libraries was mostly performed on an Illumina
461 NextSeq 500 sequencing platform, using the custom CL72 R1 sequencing primer [43] and the
462 Gesaffelstein custom index 2 sequencing primer [44], following the procedures described in [44].
463 Some *praekudarensis* libraries were additionally sequenced on an Illumina HiSeq 2500 sequencing
464 platform using the same custom primers (see Table S1).

465

466 ***Data processing***

467 Processing of the sequence reads was carried out within the BEARCAVE v.ce78f40 data analysis
468 and storage environment (available at: <https://github.com/nikolasbasler/BEARCAVE>) and is
469 reported in Table S1. BEARCAVE is freely available and can be used to obtain details of all
470 software versions and parameter settings, as well as to replicate the described analyses. Data
471 processing involved trimming adapter sequences and removing reads < 30 bp using CutAdapt [45],
472 and merging overlapping paired-end reads using FLASH [46]. The specific BEARCAVE scripts
473 used for these steps were: “*trim_merge_DS_PE_standard.sh*” for trimming and merging paired-end
474 data generated from double stranded libraries (modern and some published ancient datasets);
475 “*trim_merge_SS_PE_CL72.sh*” for trimming and merging paired-end data generated from single
476 stranded libraries (ancient datasets); and “*trim_SE.sh*” for trimming single-end data. Reads were
477 then mapped to the reference genome assemblies of the polar bear [47] and the giant panda [48]
478 using the bwa [49] aln algorithm and samtools [50], filtering for mapping quality (-q 30) and
479 potential PCR duplicates (rmdup). For the *praekudarensis* data, duplicate removal was carried out
480 separately for each library prior to merging them into a single genomic dataset. The specific
481 BEARCAVE scripts used for mapping datasets to the polar bear reference were: “*map_SE.sh*” for
482 mapping ancient datasets with default bwa parameters, excluding unmerged read-pairs from paired-
483 end datasets since they likely represent modern contamination, rendering these datasets effectively
484 single-end and “*map_modern_PE.sh*” for mapping modern datasets with default bwa parameters
485 including unmerged read pairs. The giant panda lineage is comparatively diverged from the
486 investigated clade (around 12–19 million years [51,52]), requiring relaxation of the number of
487 allowed mismatches between read and reference (-n 0.01, implemented using the corresponding
488 BEARCAVE scripts) in order to achieve acceptable mapping performance [10]. Nonetheless, we
489 were consistently able to map more data to the polar bear than the panda reference, reflecting its
490 lower divergence from the investigated samples. For this reason, subsequent analyses investigating
491 the broader scale patterns of divergence among the sampled genomes utilised the polar bear
492 mapping reference in order to maximise the number of sampled genome positions. For analyses
493 investigating patterns of admixture, the panda was used as mapping reference since these analyses
494 may be biased by using the polar bear mapping reference, which represents an ingroup to the
495 investigated clade [53,54].

496

497

498 **QUANTIFICATION AND STATISTICAL ANALYSIS**

499

500 ***Assessment of ancient DNA authenticity***

501 We assessed the authenticity of the cave bear datasets by estimating the endogenous fragment
502 length distribution and extent of cytosine deamination for 10 million randomly sampled reads
503 mapping successfully to the polar bear reference, using the program mapDamage v2.08 [55] with
504 Bayesian statistical estimation disabled and the merge reference sequences option enabled. All cave
505 bear datasets showed evidence of DNA fragmentation and cytosine deamination consistent with the
506 sample ages (Figure S1).

507

508 ***Nuclear genome PCA***

509 We investigated the broad scale patterns of divergence among the seven sampled cave bear taxa,
510 using principal components analysis (PCA) of a single representative genome of each taxon. The
511 polar bear was used as mapping reference for this analysis. A covariance matrix was calculated by
512 sampling a single nucleotide at random from the read stack at each position of the reference genome
513 using single base identity by state (IBS) in ANGSD v0.916 [56], only considering reads with a
514 minimum mapping quality score of 30 (-minMapQ 30) and nucleotides with a minimum base
515 quality score of 30 (-minQ 30). We further only considered sites from scaffolds > 1 Mb in length,
516 with no missing data (-minInd N, where N = number of individuals), and which were below the
517 upper 95th percentile of global coverage (-setMaxDepth, determined in advance using the -doDepth
518 function in angsd). Transition (identified using genotype likelihoods) and singleton ($1/N < -\text{minFreq}$
519 $< 2/N$) sites were also excluded. PCA of the covariance matrix was then carried out using the
520 “eigen” function in R [57]. The exclusion of singleton sites in this analysis is an effective way of
521 reducing sequencing errors, which frequently occur at high abundance in ancient datasets. However,
522 since private alleles are also removed, this approach is sensitive to unbalanced sampling of clades,
523 with the tendency to underestimate divergence for undersampled lineages [11]. This effect was
524 observed in preliminary analyses including both *kudarensis* individuals, since all other cave bear
525 taxa were represented by single individuals. The sampling of the *kudarensis* lineage was therefore
526 reduced to the individual with the higher coverage (HV74) in order to achieve a less biased
527 assessment of cave bear relationships. The ordination of individuals along PC1 and PC2 of this
528 analysis is shown in Figure 1A, and along PC3 to PC6 in Figure 1B.

529

530

531 ***Generation of error-reduced genome sequences***

532 We prepared two error-reduced sets of genome sequences using Consensify: one for datasets
533 mapped to the polar bear reference, which was used to estimate phylogeny and genetic distances;
534 and one for datasets mapped to the panda reference for admixture tests using D-statistics.

535

536 For the first set of Consensify sequences, for each dataset we used angsd to count the observed
537 frequency of mapped bases at each position of the polar bear reference (-doCounts function),
538 filtering for mapping (-minMapQ 30) and base calling (-minQ 30) qualities. In order to achieve the
539 most accurate estimates of genetic distances, we additionally excluded the terminal nucleotide of
540 each mapped sequence to further reduce the probability of introducing errors resulting from
541 cytosine deamination. The Consensify error-reduced sequence for each dataset was then generated
542 from these base counts using the Consensify script (available from

543 <https://github.com/jlapajmans/Consensify>), applying a maximum depth filter of the integer $< 95\%$
544 depth for each individual dataset, calculated in advance using the `-doDepth` function in `angsd`.
545 Generation of the second set of sequences used the same methodology applied to datasets mapped
546 to the panda reference, except that the terminal nucleotides of the mapped sequences were included
547 in base counts. The Consensify error reduced sequences are summarised in Table S1.

548
549

550 ***Phylogenetic analyses***

551 We estimated phylogenetic relationships among the 12 sampled nuclear genomes of cave bears,
552 brown bears and polar bears, using the Consensify error-reduced sequences generated from datasets
553 mapped to the polar bear reference. We used the ReDuCToR script (included in the Consensify
554 distribution) to combine the Consensify sequences into a single alignment, removing all invariant
555 columns and any containing missing data. Maximum-likelihood phylogenetic analysis was then
556 carried out using RaxML v8.2.12 [58] under the GTR+GAMMA substitution model with 100 rapid
557 bootstrap replicates and a thorough maximum likelihood search for the final tree (“-f a” option),
558 which was rooted using the Asiatic black bear outgroup. Bootstrap values $\geq 80\%$ were considered as
559 statistically supported. The resulting phylogeny is shown in Figure 1D.

560

561 To estimate mitochondrial relationships, the *praekudarensis* mitochondrial genome sequence was
562 generated from the datasets described in Table S1, except “6ux” and “j54”, which were sequenced
563 at a later date. Adapter trimming was performed as described above (data processing section),
564 except that reads < 28 bp were discarded. Subsequent manual inspection of the mapped reads
565 indicated that this lower minimum read length threshold was appropriate for reconstruction of the
566 *praekudarensis* mitochondrial genome. The reads were mapped to the published reference
567 mitochondrial sequence of the *kudarensis* cave bear HV74 [10] using the `bwa aln` algorithm,
568 discarding reads with MapQuality score < 30 with `samtools v1.3.1`, and removing duplicate reads
569 using `MarkReadsByStartEnd.jar` ([https://github.com/dariober/Java-](https://github.com/dariober/Java-cafe/tree/master/MarkDupsByStartEnd)
570 `cafe/tree/master/MarkDupsByStartEnd`). A consensus sequence was then generated from this
571 alignment in `Geneious v7.0`, using a minimum sequence depth of 3x and a 75% majority rule for
572 base calling. The consensus sequence was manually checked against the original alignment to
573 exclude the possibility of erroneous or incorrect consensus base calls. Details of the mitochondrial
574 genome reconstruction are shown in Table S7.

575

576 Mitochondrial genome sequences were also generated for the two brown bears (Ge, Uap), the two
577 polar bears (SRS412584, SRS412585), the Asiatic black bear (ERS781634), and four of the Late
578 Pleistocene cave bears (HV72, BO4, BO5, WK01), from the datasets described in Table S1. The
579 mitochondrial genome sequences of the brown bear Uap and *eremus* cave bear WK01 have been
580 published previously, based on much lower coverage [59]. We therefore recomputed them using the
581 higher coverage datasets of [10] in order to achieve a more complete sequence. Mitochondrial
582 reconstruction followed the methodology described above for *praekudarensis*, except that reads $<$
583 30 bp were discarded, reads from each dataset were mapped to a reference mitochondrial sequence
584 selected as a close relative of the respective taxon, and consensus sequences were generated using a
585 minimum sequence depth of 3x and a 90% majority rule for base calling. Details of the
586 mitochondrial genome reconstruction are shown in Table S7.

587

588 The consensus sequences were aligned with published sequences of the *ingressus* (GS136),
589 *spelaeus* (E-VD-1838), *eremus* (WK01) and *kudarensis* (HV74) individuals using the MUSCLE
590 algorithm [60] implemented in MEGA X [61] with default parameters. The *Ursus* control region
591 contains a microsatellite repeat which was removed as this cannot be reliably recovered using short
592 read data. Maximum likelihood phylogenetic analysis was carried out as described above for the
593 nuclear genome alignment. The resulting phylogeny is shown in Figure 1C.

594
595

596 ***Molecular dating***

597 Genomic data from individuals sampled at different time points provides information on their
598 genome-wide substitution rate. To estimate this rate for the cave, polar and brown bear clade, we
599 compared the genomic divergences of the *praekudarensis* and *kudarensis* datasets to modern polar
600 bears and brown bears, which are expected to be lower in the case of *praekudarensis* since its
601 divergence time from the clade's common ancestor is considerably less. Thus, assuming a strict
602 molecular clock, the difference in divergence divided by the median estimate of 305,400 years
603 separating *praekudarensis* and *kudarensis* provides an estimate of the per-lineage substitution rate.
604 The ReDuCToR alignment of Consensify sequences generated from datasets mapped to the polar
605 bear reference was recomputed to include invariant positions. Pairwise genomic distances were then
606 calculated from this alignment under the JC69 substitution model using the `dist.dna` function in the
607 R package "ape", considering both transitions and transversions. Assuming the sites sampled using
608 Consensify are a random and unbiased sample of the genome, these distances equate to whole
609 genome divergences and can be used to estimate the genome-wide substitution rate. Six sets of
610 substitution rate estimates were calculated using all combinations of the two *kudarensis* individuals,
611 both polar bears and the modern Georgian brown bear (Table S3). The six estimates were highly
612 consistent and their mean (9.56231×10^{-10} substitutions/site/year) was used for subsequent
613 divergence time estimations. The consistency of the rate estimates supports both the validity of our
614 method, and the assumption of a strict molecular clock. We additionally estimated the genome-wide
615 substitution rate assuming ages of the *praekudarensis* sample ± 90 ka, representing the uncertainty
616 in its radiothermoluminescence date. We also repeated this entire set of calculations using pairwise
617 mitochondrial distances to estimate the mitochondrial substitution rate.

618

619 We applied substitution rate estimates to calculate nuclear (Table S4) and mitochondrial (S5)
620 divergence times from pairwise genetic distances among all individuals. Since the estimates reflect
621 the per-lineage substitution rate, they were multiplied by two to obtain the rate of genetic
622 divergence between sister lineages, assuming a strict molecular clock. Genetic divergences between
623 individuals were then divided by this estimated rate of genetic divergence to obtain the divergence
624 time in years (Tables S4 and S5). The resulting pairwise divergence times represent the total time
625 taken for lineages to achieve the observed genetic divergence, and do not take into account the non-
626 contemporaneous ages of the individuals. The median age of each pair of individuals was therefore
627 added to their respective pairwise divergence time, which, assuming a strict molecular clock,
628 provides their absolute time of divergence before the present day (Tables S4 and S5). This
629 procedure resulted in multiple absolute age estimates for most nodes of the phylogeny, with each
630 estimate based on a different combination of individuals. As for the substitution rate estimates, the
631 consistency of these absolute node age estimates supports both the validity of our method, and the
632 assumption of a strict molecular clock. To provide the calibrated trees in Figure 3, nodes were
633 centered on the mean of their calculated median age estimates.

634

635

636 ***Comparison with other divergence estimates***

637 Based on a median radiothermoluminescence age of 360 ka for the *praekudarensis* sample, our
638 nuclear genome analysis provided an estimated divergence time of cave bears and their sister clade,
639 brown and polar bears, of 1.52 million years. The estimate provided by mitochondrial DNA is
640 remarkably similar, at 1.48 million years. These estimates coincide with the last documented fossil
641 occurrences ~1.6 million years ago of their accepted common ancestor, *Ursus etruscus* [62–64].
642 They also moderately pre-date the earliest documented fossil occurrences of the accepted ancestral
643 cave bear, *Ursus deningeri*, towards the end of the Early Pleistocene (a review of the literature is
644 provided in [65]). Finally, they moderately pre-date the earliest documented fossil showing *arctos*-
645 like characteristics, which have been assigned to the brown bear lineage. These fossils also date
646 towards the end of the Early Pleistocene, around 1.2 million years ago [63]. Our estimated
647 divergence time is also considerably younger than a previous estimate based on complete
648 mitochondrial genomes [51], which reported a divergence estimate of 2.75 million years (95%
649 credibility interval (CI) 2.1–3.57) based on fossil calibration of the seal/bear divergence and of the
650 *Ursus* lineage. A second study analysing ~4kb of mitochondrial sequence [66] utilised four
651 calibration points within the bear clade. Although the divergence time of cave bears from their sister
652 clade was not reported in this study, as first author AB carried out this analysis we can confirm the
653 estimate was 2.20 million years (95% CI 1.58–3.00 million years). In contrast, an early study [67]
654 based on control region and cytochrome b sequences produced a more recent estimate than ours,
655 around 1.2 million years.

656

657

658 ***Tests of nuclear admixture***

659 D-statistics were calculated from the Consensify error-reduced sequences generated from datasets
660 mapped to the panda reference using the published C++ program *D_stat.cpp* [10], and the results
661 processed using the python scripts *D_stat_parser.py* and *weighted_block_jackknife.py* (available
662 from <https://github.com/jacahill/Admixture>). Significance of the D-statistics was assessed by
663 calculating the standard error using a weighted block jackknife analysis using 5 Mb genome
664 windows, with D values deviating more than three standard-errors from zero (absolute Z-score > 3)
665 considered as statistically significant. These tests used the Asiatic black bear as outgroup for allele
666 polarisation, which has previously been shown to be a suitable outgroup taxon for testing for
667 admixture within the brown-polar-cave bear clade [10]. The two brown bears included in this study
668 have previously been shown to exhibit high genomic proportions of admixture with cave bears [10],
669 and were chosen to maximise sensitivity in detecting the specific admixing cave bear lineage(s).

670

671 We calculated D-statistics for all possible combinations of individuals congruent with their nuclear
672 phylogeny (Figure 1D). We found significant evidence of differential admixture between brown
673 bears and cave bears subsequent to the divergence of brown bears and polar bears; between brown
674 bears and European+Uralian cave bears subsequent to their divergence from the Caucasian cave
675 bears; and between European cave bears and the *kudarensis* lineage, subsequent to their divergence
676 from their respective sister clades, the Uralian cave bear *rossicus* and the *praekudarensis* lineage
677 (Figure 4). All other comparisons were not significantly different from zero.

678

679 **SUPPLEMENTAL ITEM TITLES**

680
681 Figure S1. Assessment of ancient DNA authenticity. Related to STAR Methods.

682
683 Table S1. Details of data processing and generation of error-reduced genome sequences. Related to
684 STAR Methods.

685
686 Table S2. Details of sample localities and ages. Related to STAR Methods.

687
688 Table S3. Nuclear and mitochondrial substitution rate estimates based on the relative difference in
689 genomic divergence of *kudarensis* (t1) and *praekudarensis* (t2) to a modern representative of the
690 brown/polar bear clade (t3). Related to Figures 2 and 3, and STAR Methods.

691
692 Table S4. Absolute times of nuclear divergence from the present day (node age) for all sample-pairs.
693 Related to Figures 2 and 3, and STAR Methods.

694
695 Table S5. Absolute times of mitochondrial divergence from the present day (node age) for all
696 sample-pairs. Related to Figures 2 and 3, and STAR Methods.

697
698 Table S6. Radiocarbon dates for Medvezhiya and Kizel cave bears used for indirect age estimates
699 for the sequenced samples. Related to STAR Methods.

700 **REFERENCES**

701

- 702 1. Hofreiter, M., Paijmans, J.L.A., Goodchild, H., Speller, C.F., Barlow, A., Fortes, G.G.,
703 Thomas, J.A., Ludwig, A., and Collins, M.J. (2015). The future of ancient DNA: Technical
704 advances and conceptual shifts. *BioEssays* 37, 284–293.
- 705 2. Cohen, K., Finney, S., Gibbard, P.L., and Fan, J.-X. (2020). The ICS International
706 Chronostratigraphic Chart (updated). *Episodes* 36, 199–204.
- 707 3. Palkopoulou, E., Lipson, M., Mallick, S., Nielsen, S., Rohland, N., Baleka, S., Karpinski, E.,
708 Ivancevic, A.M., To, T.-H., Kortschak, R.D., *et al.* (2018). A comprehensive genomic history
709 of extinct and living elephants. *Proc. Natl. Acad. Sci.* 115, E2566–E2574.
- 710 4. Meyer, M., Palkopoulou, E., Baleka, S., Stiller, M., Penkman, K.E.H., Alt, K.W., Ishida, Y.,
711 Mania, D., Mallick, S., Meijer, T., *et al.* (2017). Palaeogenomes of Eurasian straight-tusked
712 elephants challenge the current view of elephant evolution. *Elife* 6, 1–14.
- 713 5. Prüfer, K., Racimo, F., Patterson, N., Jay, F., Sankararaman, S., Sawyer, S., Heinze, A.,
714 Renaud, G., Sudmant, P.H., De Filippo, C., *et al.* (2014). The complete genome sequence of a
715 Neanderthal from the Altai Mountains. *Nature* 505, 43–49.
- 716 6. Dabney, J., Knapp, M., Glocke, I., Gansauge, M.-T., Weihmann, A., Nickel, B., Valdiosera,
717 C., García, N., Pääbo, S., Arsuaga, J.-L., *et al.* (2013). Complete mitochondrial genome
718 sequence of a Middle Pleistocene cave bear reconstructed from ultrashort DNA fragments.
719 *Proc. Natl. Acad. Sci. U. S. A.* 110, 15758–63.
- 720 7. Meyer, M., Fu, Q., Aximu-Petri, A., Glocke, I., Nickel, B., Arsuaga, J.-L., Martínez, I.,
721 Gracia, A., María Bermúdez De Castro, J., Carbonell, E., *et al.* (2013). A mitochondrial
722 genome sequence of a hominin from Sima de los Huesos. *Nature* 505, 403–406.
- 723 8. Meyer, M., Arsuaga, J.-L., de Filippo, C., Nagel, S., Aximu-Petri, A., Nickel, B., Martínez, I.,
724 Gracia, A., de Castro, J.M.B., Carbonell, E., *et al.* (2016). Nuclear DNA sequences from the
725 Middle Pleistocene Sima de los Huesos hominins. *Nature* 531, 504–507.
- 726 9. Gamba, C., Jones, E.R., Teasdale, M.D., McLaughlin, R.L., Gonzalez-Fortes, G., Mattiangeli,
727 V., Domboróczki, L., Kóvári, I., Pap, I., Anders, A., *et al.* (2014). Genome flux and stasis in a
728 five millennium transect of European prehistory. *Nat. Commun.* 5, 5257.
- 729 10. Barlow, A., Cahill, J.A., Hartmann, S., Theunert, C., Xenikoudakis, G., Fortes, G.G.,
730 Paijmans, J.L.A., Rabeder, G., Frischauf, C., Grandal-d’Anglade, A., *et al.* (2018). Partial
731 genomic survival of cave bears in living brown bears. *Nat. Ecol. Evol.* 2, 1563–1570.
- 732 11. Barlow, A., Hartmann, S., Gonzalez, J., Hofreiter, M., and Paijmans, J.L.A. (2020).
733 Consensify: A method for generating pseudohaploid genome sequences from palaeogenomic
734 datasets with reduced error rates. *Genes (Basel)*. 11.
- 735 12. Lioubine, V.P. (1998). The Acheulian Epoch in the Caucasus. [In Russian] (St. Petersburg).
- 736 13. Baryshnikov, G.F. (1998). Cave bears from the Paleolithic of the Greater Caucasus. *Illinois*
737 *State Mus. Sci. Pap.* XXVII, 69–118.

- 738 14. Baryshnikov, G.F., and Puzachenko, A.Y. (2019). Evolution and morphological variability of
739 cheek teeth in the Kudaro cave bear (*Ursus kudarensis*, Carnivora, Ursidae). [In Russian].
740 Zool. Zh. 98, 1112–1136.
- 741 15. Stiller, M., Molak, M., Prost, S., Rabeder, G., Baryshnikov, G., Rosendahl, W., Münzel, S.,
742 Bocherens, H., Grandal-d'Anglade, A., Hilpert, B., *et al.* (2014). Mitochondrial DNA
743 diversity and evolution of the Pleistocene cave bear complex. Quat. Int. 339–340, 224–231.
- 744 16. Barlow, A., Hofreiter, M., and Knapp, M. (2019). Cave bears and ancient DNA : a mutually
745 beneficial relationship. In Berichte der Geologischen Bundesanstalt, D. Nagel and N.
746 Kavcik-Graumann, eds., pp. 33–45.
- 747 17. Cahill, J.A., Green, R.E., Fulton, T.L., Stiller, M., Jay, F., Ovsyanikov, N., Salamzade, R., St.
748 John, J., Stirling, I., Slatkin, M., *et al.* (2013). Genomic evidence for island population
749 conversion resolves conflicting theories of polar bear evolution. PLoS Genet. 9, e1003345.
- 750 18. Kumar, V., Lammers, F., Bidon, T., Pfenninger, M., Kolter, L., Nilsson, M.A., and Janke, A.
751 (2017). The evolutionary history of bears is characterized by gene flow across species. Sci.
752 Rep. 7, 1–35.
- 753 19. Baryshnikov, G.F., and Puzachenko, A.Y. (2011). Craniometrical variability in the cave bears
754 (Carnivora, Ursidae): Multivariate comparative analysis. Quat. Int. 245, 350–368.
- 755 20. Baryshnikov, G.F., and Puzachenko, A.Y. (2019). Morphometry of upper cheek teeth of cave
756 bears (Carnivora, Ursidae). Boreas 48, 581–604.
- 757 21. Kurtén, B. (1976). The cave bear story. Life and death of a vanished animal. (Columbia
758 University Press).
- 759 22. Skoglund, P., Ersmark, E., Palkopoulou, E., and Dalén, L. (2015). Ancient wolf genome
760 reveals an early divergence of domestic dog ancestors and admixture into high-latitude
761 breeds. Curr. Biol. 25, 1515–1519.
- 762 23. Besenbacher, S., Hvilsom, C., Marques-Bonet, T., Mailund, T., and Schierup, M.H. (2019).
763 Direct estimation of mutations in great apes reconciles phylogenetic dating. Nat. Ecol. Evol.
764 3, 286–292.
- 765 24. Scally, A. (2016). The mutation rate in human evolution and demographic inference. Curr.
766 Opin. Genet. Dev. 41, 36–43.
- 767 25. Cronin, M.A., Amstrup, S.C., Talbot, S.L., Sage, G.K., and Amstrup, K.S. (2009). Genetic
768 variation, relatedness, and effective population size of polar bears (*Ursus maritimus*) in the
769 southern Beaufort Sea, Alaska. J. Hered. 100, 681–690.
- 770 26. De Barba, M., Waits, L.P., Garton, E.O., Genovesi, P., Randi, E., Mustoni, A., and Groff, C.
771 (2010). The power of genetic monitoring for studying demography, ecology and genetics of a
772 reintroduced brown bear population. Mol. Ecol. 19, 3938–3951.
- 773 27. Eyre-Walker, A., and Keightley, P.D. (1999). High genomic deleterious mutation rates in
774 hominids. Nature 397, 344–347.

- 775 28. Nachman, M.W., and Crowell, S.L. (2000). Estimate of the mutation rate per nucleotide in
776 humans. *Genetics* 156, 297–304.
- 777 29. Allio, R., Donega, S., Galtier, N., and Nabholz, B. (2017). Large variation in the ratio of
778 mitochondrial to nuclear mutation rate across animals: Implications for genetic diversity and
779 the use of mitochondrial DNA as a molecular marker. *Mol. Biol. Evol.* 34, 2762–2772.
- 780 30. Rieux, A., Eriksson, A., Li, M., Sobkowiak, B., Weinert, L.A., Warmuth, V., Ruiz-Linares,
781 A., Manica, A., and Balloux, F. (2014). Improved calibration of the human mitochondrial
782 clock using ancient genomes. *Mol. Biol. Evol.* 31, 2780–2792.
- 783 31. Clark, P.U., Archer, D., Pollard, D., Blum, J.D., Rial, J.A., Brovkin, V., Mix, A.C., Piasias,
784 N.G., and Roy, M. (2006). The Middle Pleistocene transition: characteristics, mechanisms,
785 and implications for long-term changes in atmospheric pCO₂. *Quat. Sci. Rev.* 25, 3150–
786 3184.
- 787 32. Gretzinger, J., Molak, M., Reiter, E., Pfrengle, S., Urban, C., Neukamm, J., Blant, M.,
788 Conard, N.J., Cupillard, C., Dimitrijević, V., *et al.* (2019). Large-scale mitogenomic analysis
789 of the phylogeography of the Late Pleistocene cave bear. *Sci. Rep.* 9, 1–11.
- 790 33. Petit, R.J., and Excoffier, L. (2009). Gene flow and species delimitation. *Trends Ecol. Evol.*
791 24, 386–393.
- 792 34. Konishi, M., and Takata, K. (2004). Impact of asymmetrical hybridization followed by sterile
793 F 1 hybrids on species replacement in *Pseudorasbora*. *Conserv. Genet.* 5, 463–474.
- 794 35. Lioubine, V.P., and Kulikov O. (1991). About the age of the most ancient Paleolithic sites of
795 the Caucasus. [In Russian]. *Sov. Archaeol.* 4, 4–6.
- 796 36. Lioubine, V.P. (2002). L'acheuléen du Caucase (Université de Liège, Service de Préhistoire).
- 797 37. Nesmeyanov S. A. (1999). Geomorphological aspects of Paleolithic paleoecology of the
798 Western Caucasus [In Russian] (Nauchny Mir, Moscow).
- 799 38. Baryshnikov, G.F. (2002). Local biochronology of Middle and Late Pleistocene mammals
800 from the Caucasus. *Russ. J. Theriol.* 1, 61–67.
- 801 39. Guérin, C., and Baryshnikov, G.F. (1987). Le rhinocéros acheuléen de la grotte de Koudaro
802 I(Géorgie, URSS) et le problème des espèces relictées du Pléistocène du Caucase. *Geobios* 20,
803 389–396.
- 804 40. Barlow, A., Fortes, G.M.G., Dalen, L., Pinhasi, R., Gasparyan, B., Rabeder, G., Frischhauf,
805 C., Paijmans, J.L.A., and Hofreiter, M. (2016). Massive influence of DNA isolation and
806 library preparation approaches on palaeogenomic sequencing data. *bioRxiv*, 075911.
- 807 41. Pinhasi, R., Fernandes, D., Sirak, K., Novak, M., Connell, S., Alpaslan-Roodenberg, S.,
808 Gerritsen, F., Moiseyev, V., Gromov, A., Raczky, P., *et al.* (2015). Optimal ancient DNA
809 yields from the inner ear part of the human petrous bone. *PLoS One* 10, e0129102.
- 810 42. Basler, N., Xenikoudakis, G., Westbury, M. V., Song, L., Sheng, G., and Barlow, A. (2017).
811 Reduction of the contaminant fraction of DNA obtained from an ancient giant panda bone.
812 *BMC Res. Notes* 10, 754.

- 813 43. Gansauge, M.-T., and Meyer, M. (2013). Single-stranded DNA library preparation for the
814 sequencing of ancient or damaged DNA. *Nat. Protoc.* 8, 737–48.
- 815 44. Paijmans, J.L.A., Baleka, S., Henneberger, K., Taron, U.H., Trinks, A., Westbury, M. V., and
816 Barlow, A. (2017). Sequencing single-stranded libraries on the Illumina NextSeq 500
817 platform. *arXiv*, 1–5.
- 818 45. Martin, M. (2011). Cutadapt removes adapter sequences from high-throughput sequencing
819 reads. *EMBnet.journal* 17, 10.
- 820 46. Magoč, T., and Salzberg, S.L. (2011). FLASH: fast length adjustment of short reads to
821 improve genome assemblies. *Bioinformatics* 27, 2957–63.
- 822 47. Li, B., Zhang, G., Willerslev, E., and Wang, J. (2011). Genomic data from the Polar Bear
823 (*Ursus maritimus*). *Gigascience* 157, <http://dx.doi.org/10.5524/100008>.
- 824 48. Hu, Y., Wu, Q., Ma, S., Ma, T., Shan, L., Wang, X., Nie, Y., Ning, Z., Yan, L., Xiu, Y., *et al.*
825 (2017). Comparative genomics reveals convergent evolution between the bamboo-eating
826 giant and red pandas. *Proc. Natl. Acad. Sci.* 114, 201613870.
- 827 49. Li, H., and Durbin, R. (2009). Fast and accurate short read alignment with Burrows-Wheeler
828 transform. *Bioinformatics* 25, 1754–60.
- 829 50. Li, H., Handsaker, B., Wysoker, A., Fennell, T., Ruan, J., Homer, N., Marth, G., Abecasis, G.,
830 and Durbin, R. (2009). The Sequence Alignment/Map format and SAMtools. *Bioinformatics*
831 25, 2078–2079.
- 832 51. Krause, J., Unger, T., Noçon, A., Malaspinas, A.-S., Kolokotronis, S.-O., Stiller, M.,
833 Soibelzon, L., Spriggs, H., Dear, P.H., Briggs, A.W., *et al.* (2008). Mitochondrial genomes
834 reveal an explosive radiation of extinct and extant bears near the Miocene-Pliocene
835 boundary. *BMC Evol. Biol.* 8, 220.
- 836 52. Abella, J., Alba, D.M., Robles, J.M., Valenciano, A., Rotgers, C., Carmona, R., Montoya, P.,
837 and Morales, J. (2012). *Kretzoiarctos* gen. nov., the oldest member of the giant panda clade.
838 *PLoS One* 7, 1–7.
- 839 53. Sheng, G.-L., Basler, N., Ji, X.-P., Paijmans, J.L.A., Alberti, F., Preick, M., Hartmann, S.,
840 Westbury, M. V., Yuan, J.-X., Jablonski, N.G., *et al.* (2019). Paleogenome reveals genetic
841 contribution of extinct giant panda to extant populations. *Curr. Biol.* 29, 1695-1700.e6.
- 842 54. Günther, T., and Nettelblad, C. (2018). The presence and impact of reference bias on
843 population genomic studies of prehistoric human populations. *PLoS Genet* 15, e1008302.
- 844 55. Ginolhac, A., Rasmussen, M., Gilbert, M.T.P., Willerslev, E., and Orlando, L. (2011).
845 mapDamage: Testing for damage patterns in ancient DNA sequences. *Bioinformatics* 27,
846 2153–2155.
- 847 56. Korneliussen, T.S., Albrechtsen, A., and Nielsen, R. (2014). Open Access ANGSD : Analysis
848 of Next Generation Sequencing Data. *BMC Bioinformatics* 15, 1–13.
- 849 57. R Core Team (2014). R: A language and environment for statistical computing. R Found.
850 Stat. Comput. Vienna, Austria. Available at: <http://www.r-project.org/>.

- 851 58. Stamatakis, A. (2014). RAxML version 8: a tool for phylogenetic analysis and post-analysis
852 of large phylogenies. *Bioinformatics* 30, 1312–1313.
- 853 59. Fortes, G.G., Grandal-d'Anglade, A., Kolbe, B., Fernandes, D., Meleg, I.N., García-Vázquez,
854 A., Pinto-Llona, A.C., Constantin, S., de Torres, T.J., Ortiz, J.E., *et al.* (2016). Ancient DNA
855 reveals differences in behaviour and sociality between brown bears and extinct cave bears.
856 *Mol. Ecol.* 25, 4907–4918.
- 857 60. Edgar, R.C. (2004). MUSCLE: multiple sequence alignment with high accuracy and high
858 throughput. *Nucleic Acids Res* 32.
- 859 61. Kumar, S., Stecher, G., Li, M., Knyaz, C., and Tamura, K. (2018). MEGA X: Molecular
860 Evolutionary Genetics Analysis across computing platforms. *Molecular Biology and*
861 *Evolution* 35, 1547–1549.
- 862 62. Rustioni, M., and Mazza, P. (1992). The genus *Ursus* in Eurasia: Dispersal events and
863 stratigraphical significance. *Riv. Ital. di Paleontol. e Stratigr. (Research Paleontol. Stratigr.*
864 *98.*
- 865 63. Rabeder, G., Pacher, M., and Withalm, G. (2010). Early Pleistocene bear remains from
866 Deutsch-Altenburg (lower Austria). *Geol. Carpathica* 61, 192.
- 867 64. Sala, B., and Masini, F. (2007). Late Pliocene and Pleistocene small mammal chronology in
868 the Italian peninsula. *Quat. Int.* 160, 4–16.
- 869 65. van Heteren, A.H., Arlegi, M., Santos, E., Arsuaga, J.L., and Gómez-Olivencia, A. (2019).
870 Cranial and mandibular morphology of Middle Pleistocene cave bears (*Ursus deningeri*):
871 implications for diet and evolution. *Hist. Biol.* 31, 485–499.
- 872 66. Sheng, G.L., Barlow, A., Cooper, A., Hou, X.D., Ji, X.P., Jablonski, N.G., Zhong, B.J., Liu,
873 H., Flynn, L.J., Yuan, J.X., *et al.* (2018). Ancient DNA from giant panda (*Ailuropoda*
874 *melanoleuca*) of south-western China reveals genetic diversity loss during the Holocene.
875 *Genes (Basel)*. 9.
- 876 67. Loreille, O., Orlando, L., Patou-Mathis, M., Philippe, M., Taberlet, P., and Hänni, C. (2001).
877 Ancient DNA analysis reveals divergence of the cave bear, *Ursus spelaeus*, and brown bear,
878 *Ursus arctos*, lineages. *Curr. Biol.* 11, 200–203.
- 879 68. Pinhasi, R., Gasparian, B., Nahapetyan, S., Bar-Oz, G., Weissbrod, L., Bruch, A.A.,
880 Hovsepyan, R., and Wilkinson, K. (2011). Middle Palaeolithic human occupation of the high
881 altitude region of Hovk-1, Armenia. *Quat. Sci. Rev.* 30, 3846–3857.
- 882 69. Pacher, M., and Stuart, A.J. (2008). Extinction chronology and palaeobiology of the cave
883 bear (*Ursus spelaeus*). *Boreas* 38, 189–206.

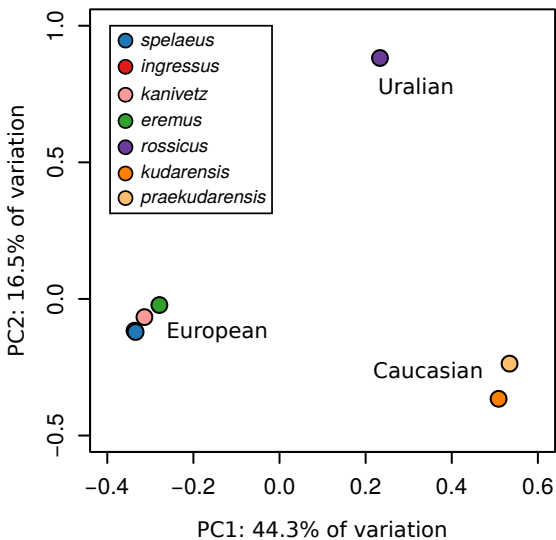
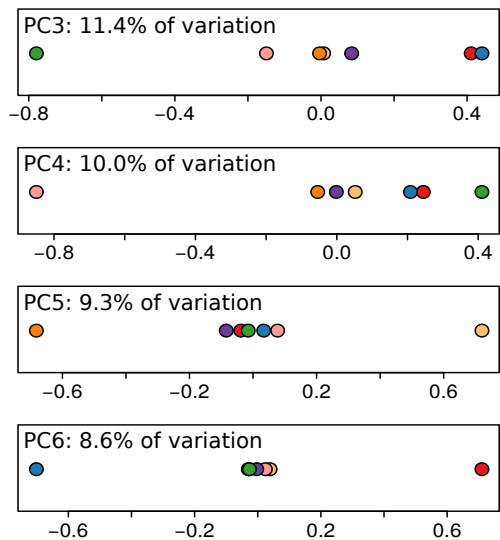
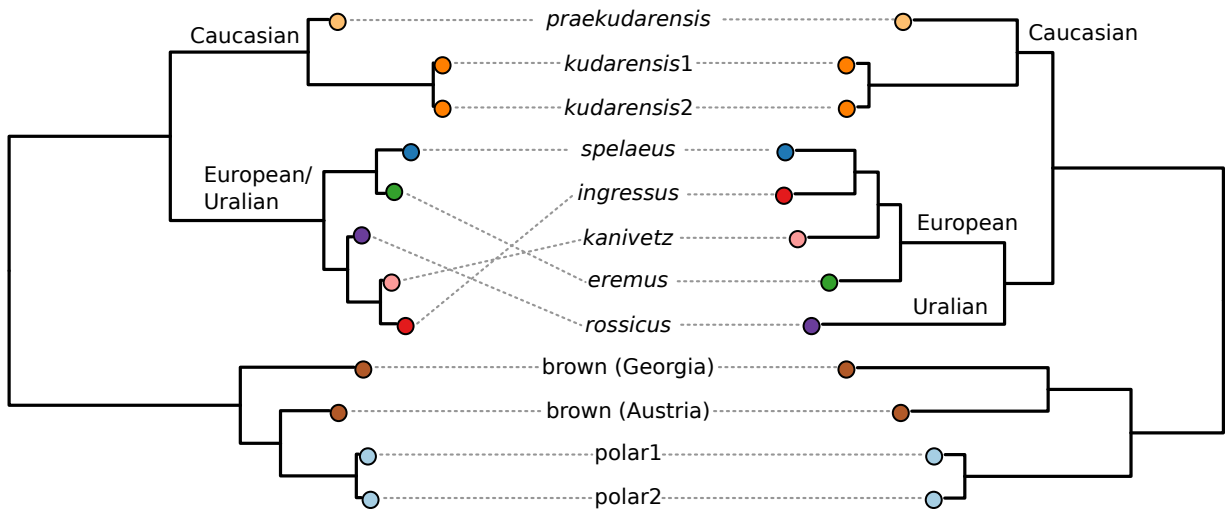
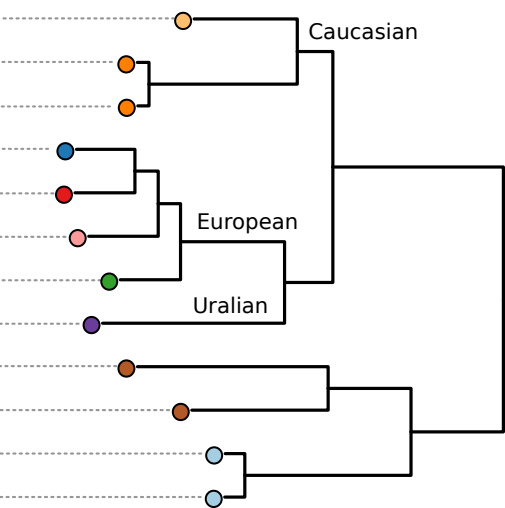
KEY RESOURCES TABLE

REAGENT or RESOURCE	SOURCE	IDENTIFIER
Chemicals, Peptides, and Recombinant Proteins		
Guanidine hydrochloride	Roth	Cat#0037.1
QIAGEN MinElute kit	Qiagen	Cat#28004
Critical Commercial Assays		
D1000 Screen Tape (Tapestation2200)	Agilent	Cat#5067-5582
dsDNA HS Assay Kit (Qubit 2.0)	Thermofisher	Cat#Q32851
Deposited Data		
7t5-KU1_1 unprocessed data, fastq format	This paper	[submitted awaiting accession]
qgj-KU1_2 unprocessed data, fastq format	This paper	[submitted awaiting accession]
ucp-KU1_2 unprocessed data, fastq format	This paper	[submitted awaiting accession]
x54-KU1_2 unprocessed data, fastq format	This paper	[submitted awaiting accession]
4z6-KU1_3 unprocessed data, fastq format	This paper	[submitted awaiting accession]
85j-KU1_3 unprocessed data, fastq format	This paper	[submitted awaiting accession]
e5e-KU1_3 unprocessed data, fastq format	This paper	[submitted awaiting accession]
vup-KU1_3 unprocessed data, fastq format	This paper	[submitted awaiting accession]
2pq-KU1_4 unprocessed data, fastq format	This paper	[submitted awaiting accession]
4id-KU1_4 unprocessed data, fastq format	This paper	[submitted awaiting accession]
65v-KU1_4 unprocessed data, fastq format	This paper	[submitted awaiting accession]
6xw-KU1_4 unprocessed data, fastq format	This paper	[submitted awaiting accession]
9s1-KU1_4 unprocessed data, fastq format	This paper	[submitted awaiting accession]
j54-KU1_4 unprocessed data, fastq format	This paper	[submitted awaiting accession]
siw-KU1_4 unprocessed data, fastq format	This paper	[submitted awaiting accession]
009-KU1_5 unprocessed data, fastq format	This paper	[submitted awaiting accession]
6mn-KU1_5 unprocessed data, fastq format	This paper	[submitted awaiting accession]
9j7-KU1_5 unprocessed data, fastq format	This paper	[submitted awaiting accession]
b3b-KU1_5 unprocessed data, fastq format	This paper	[submitted awaiting accession]
4w5-KU1_6 unprocessed data, fastq format	This paper	[submitted awaiting accession]
6ux-KU1_6 unprocessed data, fastq format	This paper	[submitted awaiting accession]
8ux-KU1_6 unprocessed data, fastq format	This paper	[submitted awaiting accession]
dLd-KU1_6 unprocessed data, fastq format	This paper	[submitted awaiting accession]
mhh-KU1_6 unprocessed data, fastq format	This paper	[submitted awaiting accession]
n3p-KU1_6 unprocessed data, fastq format	This paper	[submitted awaiting accession]

we6-KU1_6 unprocessed data, fastq format	This paper	[submitted awaiting accession]
ntw-HV72_8 unprocessed data, fastq format	This paper	[submitted awaiting accession]
w8o-HV72_8 unprocessed data, fastq format	This paper	[submitted awaiting accession]
2Ls-B05_1 unprocessed data, fastq format	This paper	[submitted awaiting accession]
vhf-B05_1 unprocessed data, fastq format	This paper	[submitted awaiting accession]
y3h-B05_1 unprocessed data, fastq format	This paper	[submitted awaiting accession]
9e1-B04_1 unprocessed data, fastq format	This paper	[submitted awaiting accession]
f9L-B04_1 unprocessed data, fastq format	This paper	[submitted awaiting accession]
vb5-B04_1 unprocessed data, fastq format	This paper	[submitted awaiting accession]
KU1 mapped reads, polar bear reference, bam format	This paper	[submitted awaiting accession]
KU1 mapped reads, panda reference, bam format	This paper	[submitted awaiting accession]
B05 mapped reads, polar bear reference, bam format	This paper	[submitted awaiting accession]
B05 mapped reads, panda reference, bam format	This paper	[submitted awaiting accession]
B04 mapped reads, polar bear reference, bam format	This paper	[submitted awaiting accession]
B04 mapped reads, panda reference, bam format	This paper	[submitted awaiting accession]
HV72 mapped reads, polar bear reference, bam format	This paper	[submitted awaiting accession]
HV72 mapped reads, panda reference, bam format	This paper	[submitted awaiting accession]
KU1 mitochondrial genome sequence	This paper	[submitted awaiting accession]
B05 mitochondrial genome sequence	This paper	[submitted awaiting accession]
B04 mitochondrial genome sequence	This paper	[submitted awaiting accession]
HV72 mitochondrial genome sequence	This paper	[submitted awaiting accession]
WK01 mitochondrial genome sequence	This paper	[submitted awaiting accession]
Oligonucleotides		
CL9 extension primer: GTGACTGGAGTTCAGACGTGTGCTCTTCCGATCT	[43]	Sigma Aldrich
Double-stranded adapter Strand 1 (CL53): CGACGCTCTTC-ddC (ddC = dideoxycytidine) Strand 2 (CL73): [Phosphate]GGAAGAGCGTCGTGTAGGGAAAGAG*T* G*T*A (* = phosphothioate linkage)	[43]	Sigma Aldrich
CL78: AGATCGGAAG[C3Spacer] ₁₀ [TEG-biotin] (TEG =triethylene glycol spacer)	[43]	Sigma Aldrich
P5 indexing primer: AATGATACGGCGACCACCGAGATCTACACnnnnnnnnA CACTCTTCCCTACACGACGCTCTT	[43]	Sigma Aldrich
P7 indexing primer: CAAGCAGAAGACGGCATACGAGATnnnnnnnnGTGAC TGGAGTTCAGACGTGT	[43]	Sigma Aldrich
IS7 amplification primer: ACACTCTTCCCTACACGAC	[43]	Sigma Aldrich

IS8 amplification primer: GTGACTGGAGTTCAGACGTGT	[43]	Sigma Aldrich
CL72 R1 sequencing primer : ACACTCTTCCCTACACGACGCTCTTCC	[43]	Sigma Aldrich
Gesaffelstein index 2 sequencing primer: GGAAGAGCGTCGTGTAGGGAAAGAGTGT	[44]	Sigma Aldrich
Software and Algorithms		
BEARCAVE ce78f40	N/A	https://github.com/nikolasbasler/BEARCAVE/
Cutadapt v1.12	[45]	https://cutadapt.readthedocs.io/en/stable/
Flash v1.2.11	[46]	https://ccb.jhu.edu/software/FLASH/
BWA v0.7.15 and v0.7.8	[49]	http://bio-bwa.sourceforge.net/
Samtools v1.3.1	[50]	https://sourceforge.net/projects/samtools/files/samtools/
PreSeq	N/A	http://smithlabresearch.org/software/preseq/
MapDamage v2.0.8	[55]	https://ginolhac.github.io/mapDamage/
ANGSD v0.916	[56]	http://www.popgen.dk/angsd
Consensify v0.1	[11]	https://github.com/jlapajmans/Consensify
ReDuCToR v0.1	[11]	https://github.com/jlapajmans/Consensify
RaxML v8.2.12	[58]	https://github.com/stamatak/standard-RAxML
R version 3.6.3	[57]	https://www.r-project.org/
MarkReadsByStartEnd.jar	N/A	https://github.com/dariober/Java-cafe/tree/master/MarkDupsByStartEnd
MEGA X v10.1.7	[61]	https://www.megasoftware.net/
D_stat.cpp	[10]	https://github.com/jacahill/Admixture
D-stat_parser.py	[10]	https://github.com/jacahill/Admixture
weighted_block_jackknife.py	[10]	https://github.com/jacahill/Admixture
Other		
Proteinase K	Promega	Cat#V3021
Zymo-spin V column extension reservoir	Zymo	Cat#C1016-50
Circligase II	Biozym	Cat#131402(CL9021K)
Endonuclease VIII	NEB	Cat#A0299S
Uracil-DNA glycosylase (Afu UDG)	NEB	Cat#M0279S
FastAP	Thermo Fisher	Cat#EF0651
MyOne C1 streptavidin beads	Thermo Fisher	Cat#65001
Bst 2.0 polymerase	NEB	Cat#M0537S

T4 DNA Polymerase	Thermo Fisher	Cat#EP0061
Buffer Tango (10x)	Thermo Fisher	Cat#BY5
T4 DNA ligase	Thermo Fisher	Cat#EL0011
Accuprime Pfx	Thermo Fisher	Cat#12344024
PEG-4000	Thermo Fisher	Cat#EP0061
Klenow fragment of DNA polymerase I	Thermo Fisher	Cat#EP0051
SYBR green PCR MasterMix	Thermo Fisher	Cat#4309155

Figure A – PCA axes 1–2**B – PCA axes 3–6****C – Mitochondrial phylogeny****D – Nuclear phylogeny**

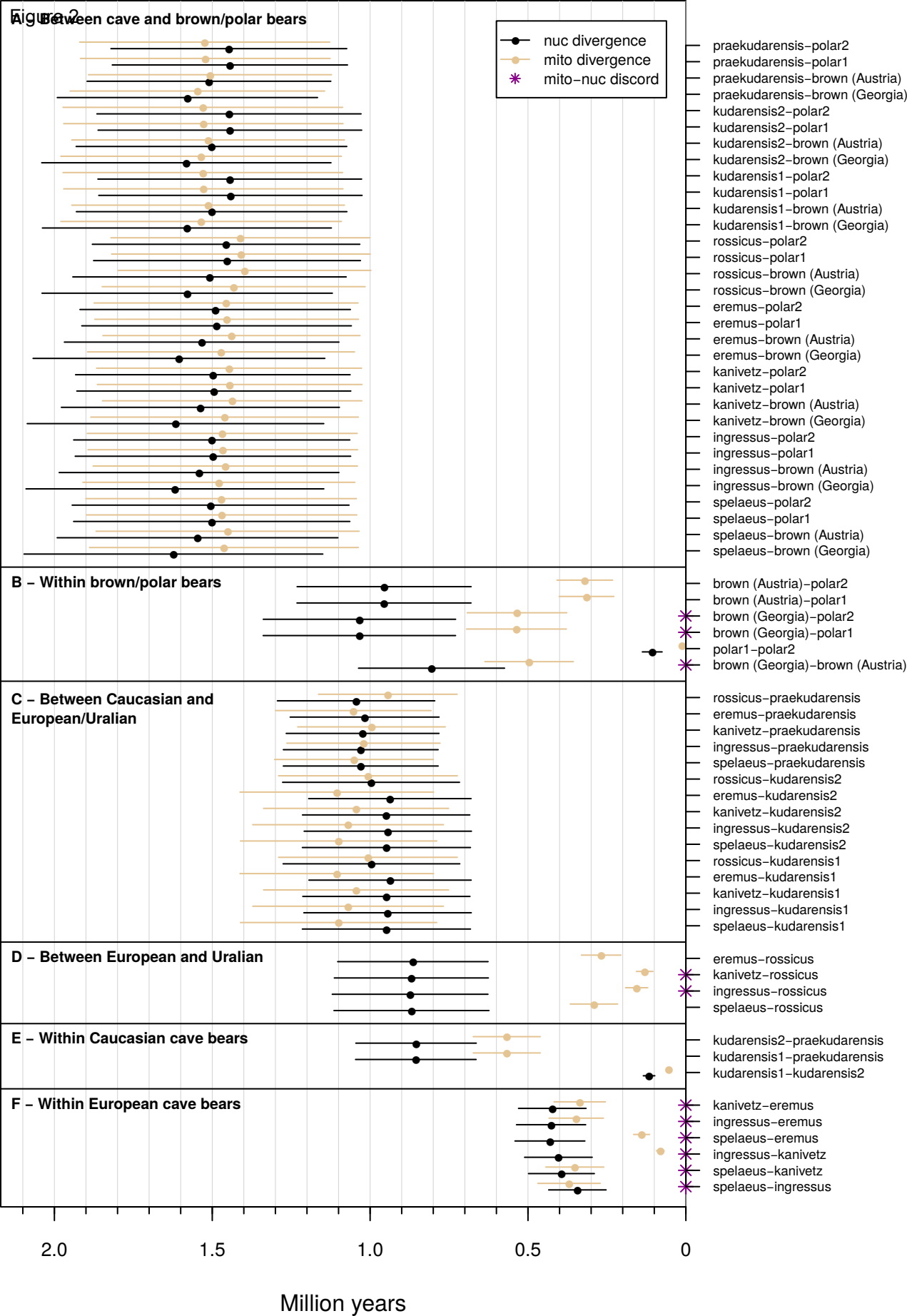
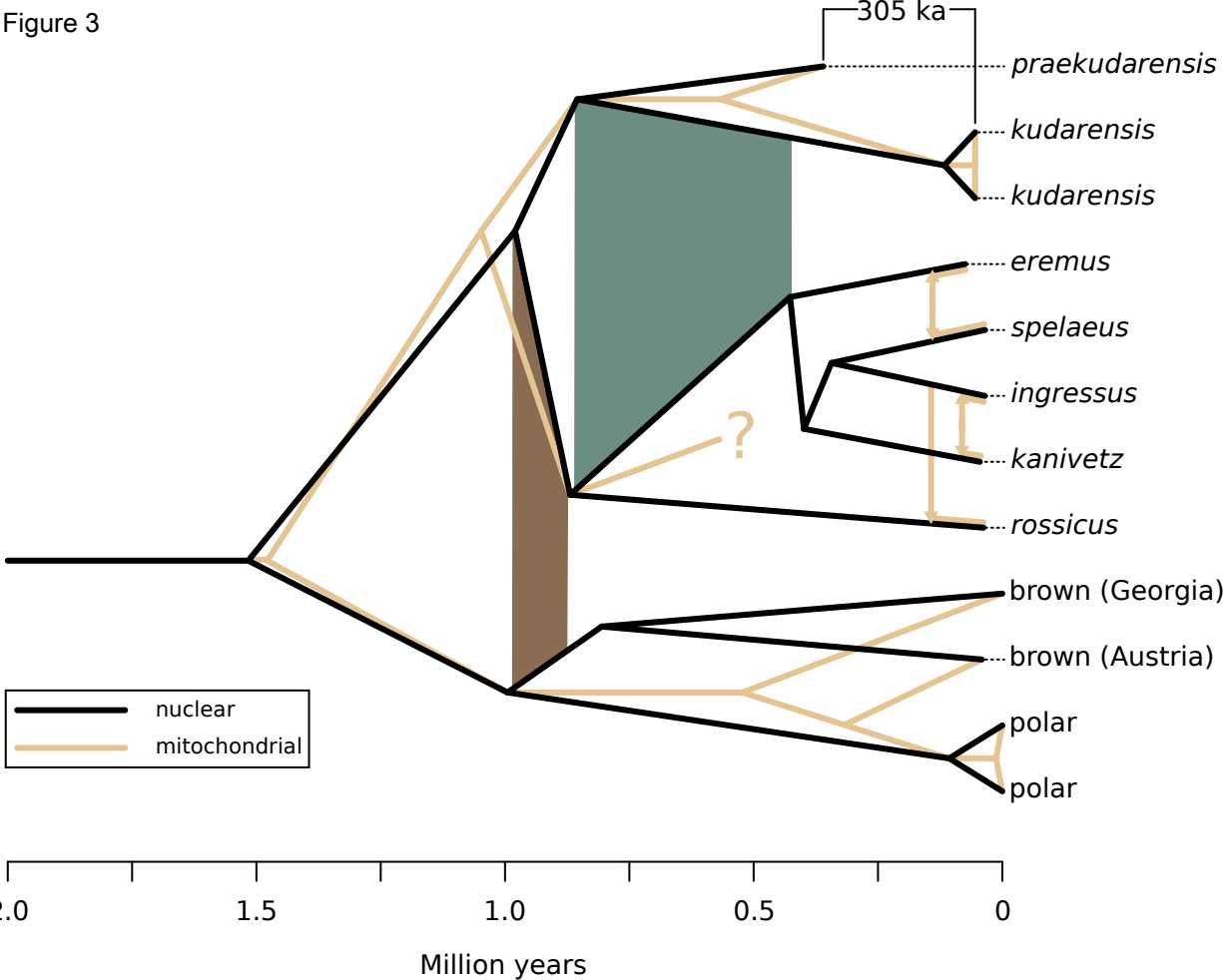
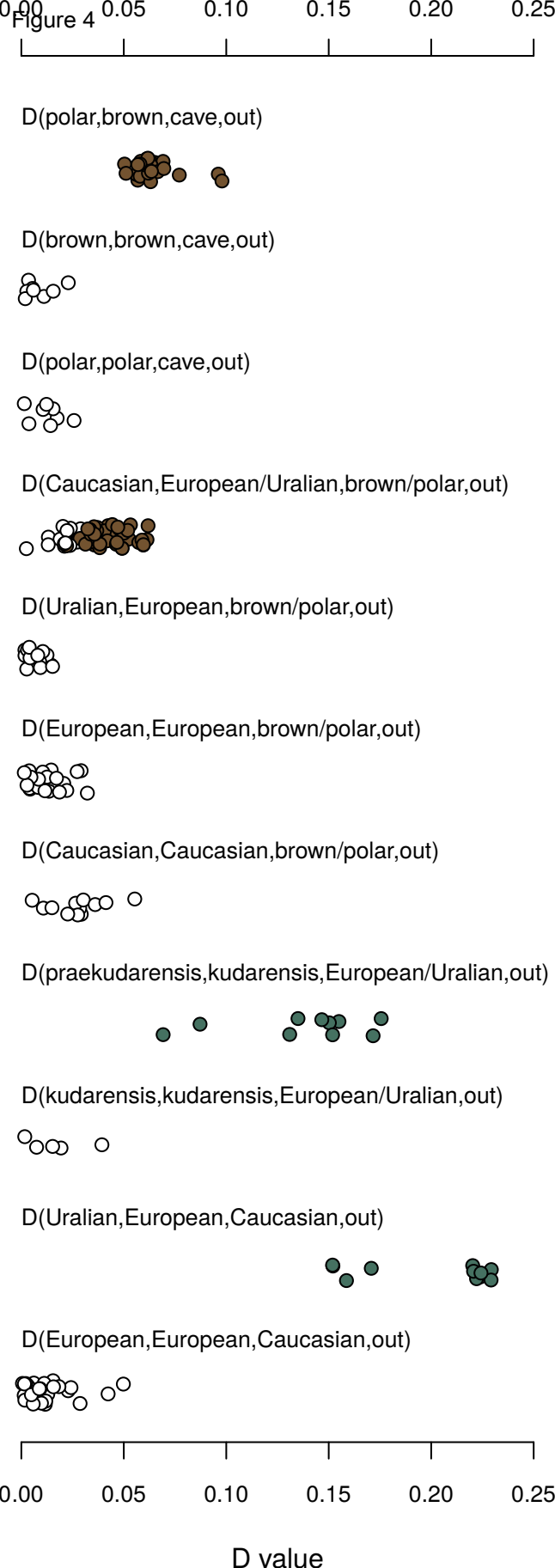


Figure 3





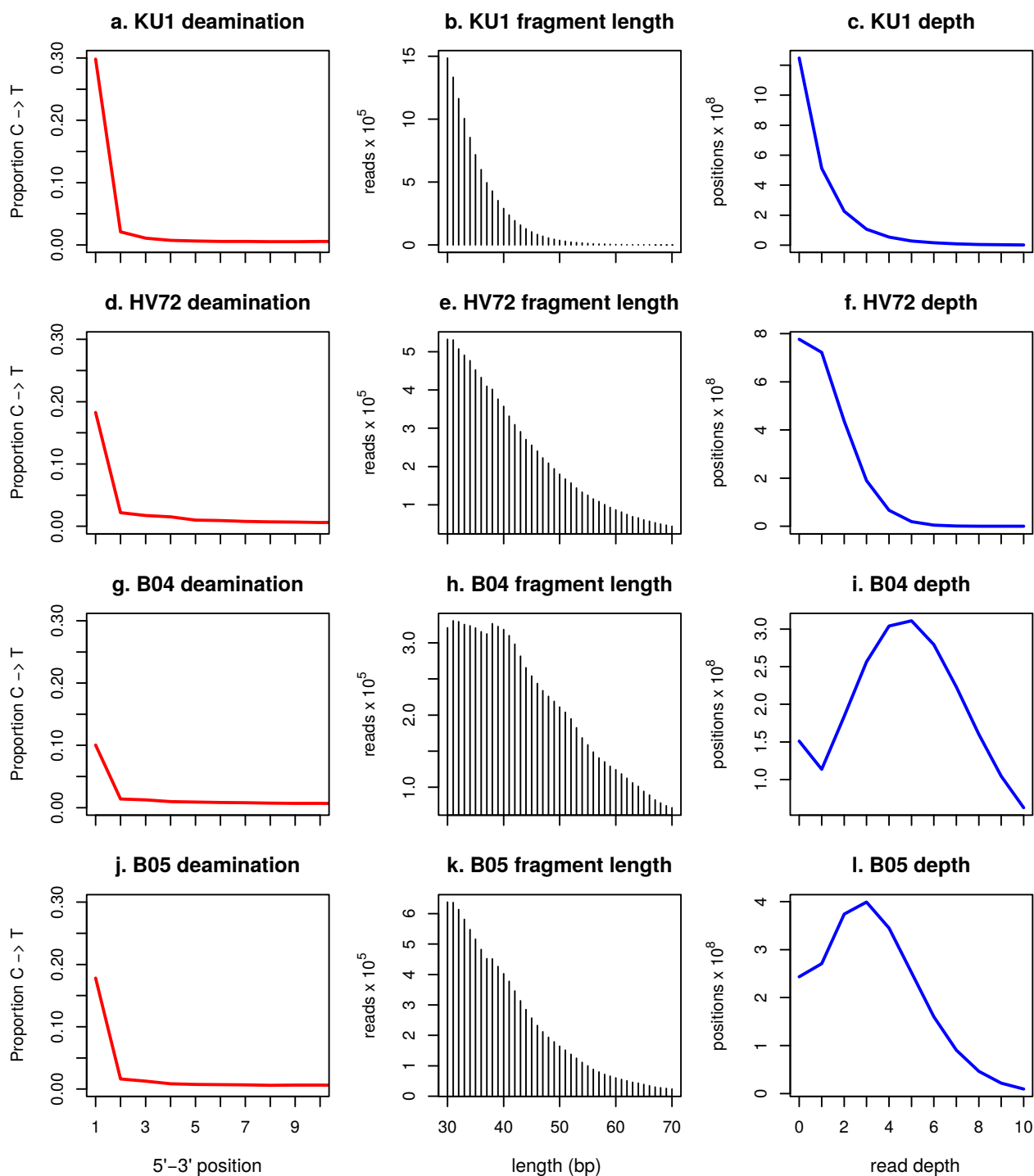


Figure S1. Assessment of ancient DNA authenticity. Related to STAR Methods.

Estimated cytosine deamination (left panels), endogenous fragment length distributions (centre panels), and mapped read depth distributions (right panels) for cave bear samples analysed in this study: KU1 *praekudarensis* (a.–c.), HV72 *kudarensis* (d.–f.), B04 *kanivetz* (g.–i.), and B05 *rossicus* (j.–l.). Cytosine deamination and fragment length distributions are estimated from 10 million mapped reads per sample. For cytosine deamination, red lines show the frequency (y axes) of thymines in reads mapped to positions where the polar bear reference poses a cytosine, for the first 10 bases of the 5' end of the sequenced fragments (x axes). The excess of C → T substitutions observed at the 5' end of the sequenced fragments indicates advanced cytosine deamination typical of ancient DNA. Note these are underestimates since the DNA extracts were treated with Endonuclease VIII to remove uracils, prior to library preparation. Endogenous fragment length

distributions represent the relative frequencies (y-axes) of reads mapping with alignment lengths between 30 bp and 70 bp (x-axes) to the polar bear reference. All distributions indicate advanced fragmentation typical of ancient DNA, with the *praekudarensis* dataset showing the greatest degree of fragmentation overall. Mapped read depth distributions show, for each complete dataset, the number (y-axes) of positions of the polar bear reference covered by 0–10 reads (x-axes).

Taxon	Run	Library	Mode ^a	Reads/read- pairs	Mapable reads ^b	Polar bear reference					Panda reference						
						Unique mapped ^c	Duplication ^d	Endogenous ^e	Mapped bp ^f	95% depth ^g bp ^h	Consensify bp ^h	Unique mapped ^c	Duplication ^d	Endogenous ^e	Mapped bp ^f	95% depth ^g bp ^h	Consensify bp ^h
<i>praekudarensis</i> (KU1) ⁱ	7f5	KU1_1	75 bp SE	929608	367745	74	0.03896	0.00020	3078			213	0.04911	0.00058	7542		
	qgj	KU1_2	75 bp SE	1376308	291063180	11981824	0.04687	0.04117	416274746			9851647	0.04562	0.03385	339757338		
	ucp		75 bp SE	392821957													
	x54		75 bp SE	129502135													
	4z6	KU1_3	75 bp SE	101656461	146383897	4355753	0.03298	0.02976	153706586			3553483	0.03193	0.02428	124381572		
	85j		75 bp SE	42946104													
	e5e		75 bp SE	1121766													
	vup		75 bp SE	49940554													
	2pq	KU1_4	75 bp SE	1373808	545309057	20008538	0.08420	0.03669	697468758			16338802	0.08286	0.02996	565343725		
	4id		75 bp SE	121346233													
	65v		75 bp SE	214714526													
	6xw		75 bp SE	44966523													
	9s1		75 bp SE	51895955													
	j54		100 bp PE	215258264													
	siw		75 bp SE	231802717													
	009	KU1_5	75 bp SE	50475622	150869957	5567830	0.03355	0.03690	194429321			4548639	0.03300	0.03015	157643168		
	6mn		75 bp SE	57832554													
	9j7		75 bp SE	134354691													
	b3b		75 bp SE	1577376													
	4w5	KU1_6	75 bp SE	42160302	508939093	17918152	0.07158	0.03521	628426966			14636130	0.07001	0.02876	509379472		
	6ux		100 bp PE	194458992													
	8ux		75 bp SE	37571245													
	dLd		75 bp SE	180488789													
	mhh		75 bp SE	196555394													
	n3p		75 bp SE	99325956													
	we6		75 bp SE	1087023													
	Total			2597540863	1642932929	59832171	0.06489	0.03642	2090309455	3	317286144	48928914	0.06357	0.02978	1696512817	3 ⁱ	275629733
<i>kudarensis</i> (HV72)	pk5	HV72_1 ^k	70 bp PE	2869873													
	nxu	HV72_2 ^l	70 bp PE	808632													
	zfb	HV72_3 ^m	70 bp PE	560954													
	et7	HV72_4 ⁿ	70 bp PE	541294													
	1oa	HV72_5 ^o	70 bp PE	617957													
	Ogw	HV72_6 ^p	70 bp PE	522654													
	xyw	HV72_7 ^q	70 bp PE	371421													
	ntw	HV72_8	75 bp SE	1978082													
	w8o	HV72_8	100 bp PE	408079285													
	Total			416350152	252663833	58829996	0.13835	0.23284	2662568631	3 ⁱ	598621119	45416300	0.13833	0.17975	2016578684	3 ⁱ	456578209
	<i>rossicus</i> (B05)	2Ls	B05_1	75 bp SE	800911												
vhf		B05_1	75 bp SE	229165973													
y3h		B05_1	75 bp SE	345021971													
Total				574988855	368057543	186891382	0.06894	0.50778	7762067882	6	1519452061	147543648	0.06852	0.40087	6056896419	6	1244838601
<i>kanivetz</i> (B04)	9e1	B04_1	75 bp SE	275211													
	f9L	B04_1	75 bp SE	236197693													
	vb5	B04_1	75 bp SE	254445960													
	Total			490918864	380166888	241762865	0.13300	0.63594	11867462564	9	1828930651	185653780	0.13037	0.48835	8981805339	8	1456996716
<i>kudarensis</i> (HV74) [S2]	Total		243461078					4990765397	4	1113055402			3760751170	4	869048390		

<i>eremus</i> (WK01) ^r [S2]	Total	499710778	7915956754	7	1569807355	6128843570	6	1210933302
<i>ingressus</i> (GS136ss) ^k [S3]	Total	432895345	9100724820	7	1659620719	6940781378	6	1266005835
<i>spelaeus</i> (E-VD-1838) ^r [S2]	Total	409117882	5818548166	5	1188238828	4552148667	5	971153181
Brown (Georgia, Ge) ^r [S2]	Total	213218024	29072595580	18	1966369913	14518303667	14	1482046107
Brown (Austria, Uap) ^r [S2]	Total	217267718	3512273973	3	767590358	2651330420	3	591504908
Polar (SRS412584) ^l [S4]	Total	105516047	12144369821	9	1704519042	6812026125	7	1118483213
Polar (SRS412585) ^l [S4]	Total	112291778	10050050358	8	1596434788	6021930179	6	1025241632
Asiatic black (ERS781634) ^r [S5]	Total	169470434	22574306140	15	1964247967	13436353408	12	1523577868

Table S1. Details of data processing and generation of error-reduced genome sequences. Related to STAR Methods.

^a75 bp single-end datasets were sequenced on the NextSeq 500 platform, 100 bp paired-end datasets were sequenced on the HiSeq 2500 platform, and 70 bp paired-end datasets were sequenced on the MiSeq platform;

^b“mapable reads” are the number of trimmed (and merged for paired-end data) reads > 30 bp used for mapping using bwa;

^cnumber of mapped reads remaining after duplicate removal;

^dproportion of mapped reads removed as duplicates;

^eestimated proportion of endogenous molecules, calculated as “unique mapped” / “mapable reads”;

^fnumber of mapped base-pairs;

^gmaximum depth filter applied for Consensify;

^htotal bp of error reduced sequence generated using Consensify;

ⁱdata from the six *praekudarensis* libraries were processed separately and then combined;

^jfor these datasets, the 95th percentile of coverage was between 2–3 reads, and so 3 reads was used as the maximum allowed depth;

^kdata from Dabney/double-stranded treatment in [S1];

^ldata from combined/double-stranded treatment in [S1];

^mdata from combined/single-stranded treatment in [S1];

ⁿdata from Dabney/double-stranded treatment in [S1];

^odata from Dabney/single-stranded treatment in [S1];

^pdata from Rohland/double-stranded treatment in [S1];

^qdata from Rohland/single-stranded treatment in [S1];

^rpublished dataset, see cited reference for details.

Sample [reference]	taxon	locality	Age (years Bp)	Dating method	Date reference
KU1 [this study]; ZIN 31896 ¹	<i>praekudarensis</i>	Kudaro-1 cave (layer 5c), South Ossetia, Southern Caucasus	360,000 ± 90,000	Layer 5c dated by Radiothermoluminescence. Also see STAR Methods.	[S7]
HV72 [this study]	<i>kudarensis1</i>	Hovk-1 cave, Armenia, Southern Caucasus	54,600 ± 5,700	Layer dated by optically stimulated luminescence	[S8]
HV74 [S2]	<i>kudarensis2</i>	Hovk-1 cave, Armenia, Southern Caucasus	54,600 ± 5,700; > 49,000	Layer dated by optically stimulated luminescence; radiocarbon dating	[S8,S1]
B05 [this study] ZIN 28601-9a/51 ¹	<i>rossicus</i>	Kizel cave, Ural Mountains, Russia	37,698 (indirect estimate)	Median of available radiocarbon dates for Kizel cave bears. See Table S6.	This study
WK01 [S2]	<i>eremus</i>	Windischkopf cave, Austria	71,992 (95% CI 54,640– 91,860)	Mitochondrial tip dating	[S6]
B04 [this study] ZIN n/n ¹	<i>kanivetz</i>	Medvezhiya cave, Ural Mountains, Russia	45,043 (indirect estimate)	Median of available radiocarbon dates for Medvezhiya cave bears. See Table S6.	This study
GS136 [S2]	<i>ingressus</i>	Gamssulzen cave, Austria	35,062 ± 966	Radiocarbon dating	[S6]
E-VD-1838 [S2]	<i>spelaeus</i>	Eiros cave, Spain	34,806 ± 931	Radiocarbon dating	[S6]
Ge [S2]	brown	Georgia, Great Caucasus	Modern	N/A	[S2]
Uap [S2]	brown	Winden cave, Austria	41,201 ± 895	Radiocarbon dating	[S6]
SRS412584 ² [S4]	polar1	North Beaufort Sea	Modern	N/A	[S4]
SRS412585 ² [S4]	polar2	Wrangel Island	Modern	N/A	[S4]
ERS781634 ² [S5]	Asiatic black	Zoo	Modern	N/A	[S5]

Table S2. Details of sample localities and ages. Related to STAR Methods.

¹Zoological Institute RAS Collection Number.

²Sample code is European Nucleotide Archive accession number.

t1	t2	t3	Divergence t1:t3 ^a	Divergence t2:t3 ^a	t1:t3 – t2:t3 ^a	median sub rate	min sub rate	max sub rate
<u>Nuclear DNA</u>								
HV72	KU1	Brown (Ge)	2.97016 x 10 ⁻³	2.67496 x 10 ⁻³	2.95198 x 10 ⁻⁴	9.66596 x 10 ⁻¹⁰	7.46581 x 10 ⁻¹⁰	1.37047 x 10 ⁻⁹
HV72	KU1	Polar (SRS412584)	2.70656 x 10 ⁻³	2.41774 x 10 ⁻³	2.88822 x 10 ⁻⁴	9.45718 x 10 ⁻¹⁰	7.30456 x 10 ⁻¹⁰	1.34086 x 10 ⁻⁹
HV72	KU1	Polar (SRS412585)	2.71051 x 10 ⁻³	2.42401 x 10 ⁻³	2.86501 x 10 ⁻⁴	9.38116 x 10 ⁻¹⁰	7.24584 x 10 ⁻¹⁰	1.33009 x 10 ⁻⁹
HV74	KU1	Brown (Ge)	2.97341 x 10 ⁻³	2.67496 x 10 ⁻³	2.98453 x 10 ⁻⁴	9.77253 x 10 ⁻¹⁰	7.54813 x 10 ⁻¹⁰	1.38558 x 10 ⁻⁹
HV74	KU1	Polar (SRS412584)	2.70982 x 10 ⁻³	2.41774 x 10 ⁻³	2.92076 x 10 ⁻⁴	9.56371 x 10 ⁻¹⁰	7.38684 x 10 ⁻¹⁰	1.35597 x 10 ⁻⁹
HV74	KU1	Polar (SRS412585)	2.71516 x 10 ⁻³	2.42401 x 10 ⁻³	2.91149 x 10 ⁻⁴	9.53335 x 10 ⁻¹⁰	7.36339 x 10 ⁻¹⁰	1.35166 x 10 ⁻⁹
Mean						9.56231 x 10⁻¹⁰	7.38576 x 10⁻¹⁰	1.35577 x 10⁻⁹
<u>Mitochondrial DNA</u>								
HV72	KU1	Brown (Ge)	5.46936 x 10 ⁻²	4.95862 x 10 ⁻²	5.10732 x 10 ⁻³	1.67234 x 10 ⁻⁸	1.29168 x 10 ⁻⁸	2.37109 x 10 ⁻⁸
HV72	KU1	Polar (SRS412584)	5.44350 x 10 ⁻²	4.86811 x 10 ⁻²	5.75381 x 10 ⁻³	1.88403 x 10 ⁻⁸	1.45519 x 10 ⁻⁸	2.67122 x 10 ⁻⁸
HV72	KU1	Polar (SRS412585)	5.44996 x 10 ⁻²	4.87458 x 10 ⁻²	5.75381 x 10 ⁻³	1.88403 x 10 ⁻⁸	1.45519 x 10 ⁻⁸	2.67122 x 10 ⁻⁸
HV74	KU1	Brown (Ge)	5.46936 x 10 ⁻²	4.95862 x 10 ⁻²	5.10732 x 10 ⁻³	1.67234 x 10 ⁻⁸	1.29168 x 10 ⁻⁸	2.37109 x 10 ⁻⁸
HV74	KU1	Polar (SRS412584)	5.44350 x 10 ⁻²	4.86811 x 10 ⁻²	5.75381 x 10 ⁻³	1.88403 x 10 ⁻⁸	1.45519 x 10 ⁻⁸	2.67122 x 10 ⁻⁸
HV74	KU1	Polar (SRS412585)	5.44996 x 10 ⁻²	4.87458 x 10 ⁻²	5.75381 x 10 ⁻³	1.88403 x 10 ⁻⁸	1.45519 x 10 ⁻⁸	2.67122 x 10 ⁻⁸
Mean						1.81346 x 10⁻⁸	1.40069 x 10⁻⁸	2.57118 x 10⁻⁸

Table S3. Nuclear and mitochondrial substitution rate estimates based on the relative difference in genomic divergence of *kudarensis* (t1) and *praekudarensis* (t2) to a modern representative of the brown/polar bear clade (t3). Related to Figures 2 and 3, and STAR Methods.

^aValues are the genetic divergence measured as the proportion of positions in the ReDuCToR alignment.

t1	t2	Age t1	Age t2	Genetic divergence	Divergence Time	Median node age	min node age	max node age
spelaeus	ingressus	34806	35062	5.90264×10^{-4}	308641	343575	252620	434530
spelaeus	kanivetz	34806	45043	6.77406×10^{-4}	354206	394131	289748	498514
ingressus	kanivetz	35062	45043	6.95485×10^{-4}	363659	403712	296543	510881
spelaeus	eremus	34806	74696	7.18663×10^{-4}	375779	430530	319790	541270
ingressus	eremus	35062	74696	7.11478×10^{-4}	372022	426901	317268	536534
kanivetz	eremus	45043	74696	6.94558×10^{-4}	363175	423044	316018	530070
spelaeus	rossicus	34806	37698	1.59278×10^{-3}	832844	869096	623661	1114532
ingressus	rossicus	35062	37698	1.60067×10^{-3}	836970	873350	626699	1120001
kanivetz	rossicus	45043	37698	1.58373×10^{-3}	828112	869482	625442	1113523
eremus	rossicus	74696	37698	1.54614×10^{-3}	808455	864652	626404	1102901
kudarensis (HV72)	kudarensis (HV74)	54600	54600	1.18571×10^{-4}	61999	116599	98328	134870
kudarensis (HV72)	praekudarensis	54600	360000	1.23921×10^{-3}	647965	855265	664313	1046218
kudarensis (HV74)	praekudarensis	54600	360000	1.23782×10^{-3}	647237	854537	663799	1045275
spelaeus	kudarensis (HV72)	34806	54600	1.72832×10^{-3}	903713	948416	682096	1214736
ingressus	kudarensis (HV72)	35062	54600	1.72112×10^{-3}	899951	944782	679571	1209994
kanivetz	kudarensis (HV72)	45043	54600	1.71880×10^{-3}	898737	948559	683705	1213413
eremus	kudarensis (HV72)	74696	54600	1.66821×10^{-3}	872282	936930	679872	1193987
rossicus	kudarensis (HV72)	37698	54600	1.81629×10^{-3}	949712	995861	715985	1275737
spelaeus	kudarensis (HV74)	34806	54600	1.72832×10^{-3}	903713	948416	682096	1214736
ingressus	kudarensis (HV74)	35062	54600	1.71973×10^{-3}	899223	944054	679057	1209051
kanivetz	kudarensis (HV74)	45043	54600	1.72019×10^{-3}	899466	949287	684219	1214356
eremus	kudarensis (HV74)	74696	54600	1.66913×10^{-3}	872767	937415	680215	1194616
rossicus	kudarensis (HV74)	37698	54600	1.81861×10^{-3}	950926	997075	716841	1277309
spelaeus	praekudarensis	34806	360000	1.59186×10^{-3}	832359	1029762	784469	1275054
ingressus	praekudarensis	35062	360000	1.59162×10^{-3}	832237	1029768	784512	1275025
kanivetz	praekudarensis	45043	360000	1.57074×10^{-3}	821317	1023838	781800	1265877
eremus	praekudarensis	74696	360000	1.53013×10^{-3}	800084	1017432	781651	1253213
rossicus	praekudarensis	37698	360000	1.61738×10^{-3}	845706	1044555	795330	1293781
brown (Ge)	Brown (Uap)	0	41201	1.50113×10^{-3}	784918	805518	574206	1036830
Polar (SRS412584)	Polar (SRS412585)	0	0	2.03806×10^{-4}	106567	106567	75162	137972
brown (Ge)	Polar (SRS412584)	0	0	1.97764×10^{-3}	1034078	1034078	729340	1338816
brown (Ge)	Polar (SRS412585)	0	0	1.97717×10^{-3}	1033835	1033835	729169	1338502
Brown (Uap)	Polar (SRS412584)	41201	0	1.78913×10^{-3}	935511	956112	680421	1231803
Brown (Uap)	Polar (SRS412585)	41201	0	1.78843×10^{-3}	935147	955748	680164	1231332
spelaeus	brown (Ge)	34806	0	3.07060×10^{-3}	1605572	1622975	1149820	2096130
spelaeus	Brown (Uap)	34806	41201	2.88530×10^{-3}	1508685	1546688	1102086	1991291
spelaeus	Polar (SRS412584)	34806	0	2.83881×10^{-3}	1484376	1501779	1064340	1939218
spelaeus	Polar (SRS412585)	34806	0	2.84555×10^{-3}	1487900	1505303	1066826	1943781
ingressus	brown (Ge)	35062	0	3.06130×10^{-3}	1600709	1618240	1146518	2089961
ingressus	Brown (Uap)	35062	41201	2.87577×10^{-3}	1503701	1541833	1098699	1984967
ingressus	Polar (SRS412584)	35062	0	2.83114×10^{-3}	1480365	1497896	1061639	1934153
ingressus	Polar (SRS412585)	35062	0	2.83835×10^{-3}	1484133	1501664	1064296	1939031
kanivetz	brown (Ge)	45043	0	3.04828×10^{-3}	1593900	1616422	1146707	2086137
kanivetz	Brown (Uap)	45043	41201	2.85811×10^{-3}	1494464	1537586	1097174	1977998
kanivetz	Polar (SRS412584)	45043	0	2.81627×10^{-3}	1472586	1495108	1061143	1929072
kanivetz	Polar (SRS412585)	45043	0	2.82208×10^{-3}	1475625	1498146	1063286	1933006
eremus	brown (Ge)	74696	0	2.99898×10^{-3}	1568127	1605475	1143355	2067595
eremus	Brown (Uap)	74696	41201	2.82208×10^{-3}	1475625	1533573	1098713	1968433
eremus	Polar (SRS412584)	74696	0	2.77118×10^{-3}	1449009	1486357	1059340	1913373
eremus	Polar (SRS412585)	74696	0	2.77954×10^{-3}	1453384	1490732	1062426	1919037
rossicus	brown (Ge)	37698	0	2.98457×10^{-3}	1560590	1579439	1119540	2039338
rossicus	Brown (Uap)	37698	41201	2.80999×10^{-3}	1469305	1508754	1075757	1941752
rossicus	Polar (SRS412584)	37698	0	2.74328×10^{-3}	1434425	1453274	1030556	1875993
rossicus	Polar (SRS412585)	37698	0	2.74910×10^{-3}	1437463	1456312	1032698	1879926
kudarensis (HV72)	brown (Ge)	54600	0	2.97016×10^{-3}	1553053	1580353	1122675	2038031
kudarensis (HV72)	Brown (Uap)	54600	41201	2.78094×10^{-3}	1454113	1502013	1073493	1930534
kudarensis (HV72)	Polar (SRS412584)	54600	0	2.70656×10^{-3}	1415224	1442524	1025464	1859585
kudarensis (HV72)	Polar (SRS412585)	54600	0	2.71051×10^{-3}	1417290	1444590	1026921	1862259
kudarensis (HV74)	brown (Ge)	54600	0	2.97341×10^{-3}	1554755	1582055	1123876	2040234
kudarensis (HV74)	Brown (Uap)	54600	41201	2.78187×10^{-3}	1454599	1502500	1073836	1931163
kudarensis (HV74)	Polar (SRS412584)	54600	0	2.70982×10^{-3}	1416926	1444226	1026664	1861787
kudarensis (HV74)	Polar (SRS412585)	54600	0	2.71516×10^{-3}	1419721	1447021	1028635	1865406
praekudarensis	brown (Ge)	360000	0	2.67496×10^{-3}	1398698	1578698	1166508	1990888
praekudarensis	Brown (Uap)	360000	41201	2.50510×10^{-3}	1309880	1510481	1124465	1896496
praekudarensis	Polar (SRS412584)	360000	0	2.41774×10^{-3}	1264203	1444203	1071648	1816758
praekudarensis	Polar (SRS412585)	360000	0	2.42401×10^{-3}	1267483	1447483	1073962	1821005

Table S4. Absolute times of nuclear divergence from the present day (node age) for all sample-pairs. Related to Figures 2 and 3, and STAR Methods.

Node ages between pairs of individuals (t1, t2) are calculated from their pairwise divergence time (genetic divergence/estimated divergence rate) combined with their respective ages (Age t1, Age t2). Median, maximum and minimum node ages are calculated, respectively, from their corresponding substitution rate estimates shown in Table S3.

t1	t2	Age t1	Age t2	Genetic divergence	Divergence Time	Median node age	Lower node age	Upper node age
spelaeus	ingressus	34806	35062	1.21541 × 10 ⁻²	335108	370042	271287	468797
spelaeus	kanivetz	34806	45043	1.13137 × 10 ⁻²	311936	351860	259934	443786
ingressus	kanivetz	35062	45043	1.48694 × 10 ⁻³	40997	81050	68968	93131
spelaeus	eremus	34806	74696	3.10318 × 10 ⁻³	85560	140311	115097	165525
ingressus	eremus	35062	74696	1.06025 × 10 ⁻²	292328	347207	261060	433355
kanivetz	eremus	45043	74696	1.00207 × 10 ⁻²	276286	336155	254735	417576
spelaeus	rossicus	34806	37698	9.24489 × 10 ⁻³	254896	291148	216031	366265
ingressus	rossicus	35062	37698	4.33152 × 10 ⁻³	119427	155807	120612	191001
kanivetz	rossicus	45043	37698	3.23248 × 10 ⁻³	89125	130495	104230	156760
eremus	rossicus	74696	37698	7.69330 × 10 ⁻³	212116	268313	205804	330823
kudarensis (HV72)	kudarensis (HV74)	54600	54600	0	0	54600	54600	54600
kudarensis (HV72)	praekudarensis	54600	360000	1.30592 × 10 ⁻²	360063	567363	461254	673472
kudarensis (HV74)	praekudarensis	54600	360000	1.30592 × 10 ⁻²	360063	567363	461254	673472
spelaeus	kudarensis (HV72)	34806	54600	3.82726 × 10 ⁻²	1055234	1099937	788964	1410910
ingressus	kudarensis (HV72)	35062	54600	3.71735 × 10 ⁻²	1024932	1069763	767720	1371806
kanivetz	kudarensis (HV72)	45043	54600	3.60745 × 10 ⁻²	994630	1044451	751338	1337564
eremus	kudarensis (HV72)	74696	54600	3.77554 × 10 ⁻²	1040974	1105622	798852	1412393
rossicus	kudarensis (HV72)	37698	54600	3.48461 × 10 ⁻²	960762	1006911	723779	1290044
spelaeus	kudarensis (HV74)	34806	54600	3.82726 × 10 ⁻²	1055234	1099937	788964	1410910
ingressus	kudarensis (HV74)	35062	54600	3.71735 × 10 ⁻²	1024932	1069763	767720	1371806
kanivetz	kudarensis (HV74)	45043	54600	3.60745 × 10 ⁻²	994630	1044451	751338	1337564
eremus	kudarensis (HV74)	74696	54600	3.77554 × 10 ⁻²	1040974	1105622	798852	1412393
rossicus	kudarensis (HV74)	37698	54600	3.48461 × 10 ⁻²	960762	1006911	723779	1290044
spelaeus	praekudarensis	34806	360000	3.09672 × 10 ⁻²	853813	1051216	799601	1302831
ingressus	praekudarensis	35062	360000	2.98681 × 10 ⁻²	823511	1021042	778357	1263726
kanivetz	praekudarensis	45043	360000	2.87691 × 10 ⁻²	793208	995730	761975	1229485
eremus	praekudarensis	74696	360000	3.03207 × 10 ⁻²	835988	1053336	806974	1299698
rossicus	praekudarensis	37698	360000	2.70235 × 10 ⁻²	745081	943930	724358	1163502
brown (Ge)	Brown (Uap)	0	41201	1.72614 × 10 ⁻²	475925	496525	356272	636778
Polar (SRS412584)	Polar (SRS412585)	0	0	4.52547 × 10 ⁻⁴	12477	12477	8800	16154
brown (Ge)	Polar (SRS412584)	0	0	1.94595 × 10 ⁻²	536530	536530	378417	694642
brown (Ge)	Polar (SRS412585)	0	0	1.93949 × 10 ⁻²	534747	534747	377160	692335
Brown (Uap)	Polar (SRS412584)	41201	0	1.06672 × 10 ⁻²	294111	314711	228038	401385
Brown (Uap)	Polar (SRS412585)	41201	0	1.08611 × 10 ⁻²	299458	320059	231810	408308
spelaeus	brown (Ge)	34806	0	5.24308 × 10 ⁻²	1445600	1463003	1036991	1889014
spelaeus	Brown (Uap)	34806	41201	5.12671 × 10 ⁻²	1413515	1451518	1034962	1868075
spelaeus	Polar (SRS412584)	34806	0	5.26894 × 10 ⁻²	1452730	1470133	1042020	1898245
spelaeus	Polar (SRS412585)	34806	0	5.27541 × 10 ⁻²	1454512	1471915	1043277	1900553
ingressus	brown (Ge)	35062	0	5.30127 × 10 ⁻²	1461642	1479173	1048434	1909912
ingressus	Brown (Uap)	35062	41201	5.15257 × 10 ⁻²	1420645	1458776	1040119	1877434
ingressus	Polar (SRS412584)	35062	0	5.25601 × 10 ⁻²	1449165	1466696	1039633	1893758
ingressus	Polar (SRS412585)	35062	0	5.26248 × 10 ⁻²	1450947	1468478	1040891	1896066
kanivetz	brown (Ge)	45043	0	5.21722 × 10 ⁻²	1438470	1460991	1037081	1884902
kanivetz	Brown (Uap)	45043	41201	5.05560 × 10 ⁻²	1393907	1437029	1026251	1847808
kanivetz	Polar (SRS412584)	45043	0	5.15904 × 10 ⁻²	1422427	1444949	1025766	1864132
kanivetz	Polar (SRS412585)	45043	0	5.16550 × 10 ⁻²	1424210	1446731	1027023	1866439
eremus	brown (Ge)	74696	0	5.20429 × 10 ⁻²	1434905	1472253	1049393	1895113
eremus	Brown (Uap)	74696	41201	5.01034 × 10 ⁻²	1381430	1439378	1032277	1846480
eremus	Polar (SRS412584)	74696	0	5.13964 × 10 ⁻²	1417080	1454428	1036821	1872035
eremus	Polar (SRS412585)	74696	0	5.14611 × 10 ⁻²	1418862	1456210	1038078	1874343
rossicus	brown (Ge)	37698	0	5.12671 × 10 ⁻²	1413515	1432364	1015807	1848920
rossicus	Brown (Uap)	37698	41201	4.92630 × 10 ⁻²	1358258	1397707	997435	1797979
rossicus	Polar (SRS412584)	37698	0	5.04267 × 10 ⁻²	1390342	1409191	999464	1818919
rossicus	Polar (SRS412585)	37698	0	5.04913 × 10 ⁻²	1392125	1410974	1000721	1821227
kudarensis (HV72)	brown (Ge)	54600	0	5.46936 × 10 ⁻²	1507987	1535287	1090890	1979684
kudarensis (HV72)	Brown (Uap)	54600	41201	5.31420 × 10 ⁻²	1465207	1513108	1081318	1944897
kudarensis (HV72)	Polar (SRS412584)	54600	0	5.44350 × 10 ⁻²	1500857	1528157	1085861	1970453
kudarensis (HV72)	Polar (SRS412585)	54600	0	5.44996 × 10 ⁻²	1502639	1529939	1087118	1972760
kudarensis (HV74)	brown (Ge)	54600	0	5.46936 × 10 ⁻²	1507987	1535287	1090890	1979684
kudarensis (HV74)	Brown (Uap)	54600	41201	5.31420 × 10 ⁻²	1465207	1513108	1081318	1944897
kudarensis (HV74)	Polar (SRS412584)	54600	0	5.44350 × 10 ⁻²	1500857	1528157	1085861	1970453
kudarensis (HV74)	Polar (SRS412585)	54600	0	5.44996 × 10 ⁻²	1502639	1529939	1087118	1972760
praekudarensis	brown (Ge)	360000	0	4.95862 × 10 ⁻²	1367170	1547170	1144271	1950069
praekudarensis	Brown (Uap)	360000	41201	4.73882 × 10 ⁻²	1306565	1507166	1122127	1892205
praekudarensis	Polar (SRS412584)	360000	0	4.86811 × 10 ⁻²	1342215	1522215	1126670	1917760
praekudarensis	Polar (SRS412585)	360000	0	4.87458 × 10 ⁻²	1343998	1523998	1127928	1920068

Table S5. Absolute times of mitochondrial divergence from the present day (node age) for all sample-pairs. Related to Figures 2 and 3, and STAR Methods.

Node ages between pairs of individuals (t1, t2) are calculated from their pairwise divergence time (genetic divergence/estimated divergence rate) combined with their respective ages (Age t1, Age t2). Median, maximum and minimum node ages are calculated, respectively, from their corresponding substitution rate estimates shown in Table S3.

Sample	Cave	ZIN cat #	Description	Date code	radiocarbon age	Delta 13C	Maximum calibrated age*	Minimum calibrated age*	Calibrated median age*	Notes
USP-01	Medvezhiya	34991-6	<i>kanivetz</i> partial skull	OxA-19568	45,150 ± 600	-20.84	47,984	45,320	46,652	Date may extend out of calibration range
USP-03	Medvezhiya	34991-19	<i>kanivetz</i> mandible	OxA-19608	42,000 ± 450	-20.1	44,251	42,616	43,434	
UKZ-05	Kizel	28601-44	<i>rossicus</i> right maxilla	OxA-19565	46,250 ± 700	-20.94	...	46,332	...	Date may extend out of calibration range
UKZ-06	Kizel	28601-32	<i>rossicus</i> right maxilla	OxA-19566	39,040 ± 330	-22.68	41,461	40,452	40,957	
-	Kizel	-	-	OxA-16964	36,390 ± 270	-21.842	39,646	38,462	39,054	From [S9]
UKZ-01	Kizel	28601-29	<i>rossicus</i> right maxilla	OxA-19561	35,330 ± 220	-21.55	38,543	37,387	37,965	
UKZ-02	Kizel	28601-13a	<i>rossicus</i> right maxilla	OxA-19562	35,110 ± 230	-21.08	38,301	37,095	37,698	
UKZ-07	Kizel	28601-41	<i>rossicus</i> right maxilla	OxA-19567	34,610 ± 230	-21.43	37,752	36,646	37,199	
UKZ-04	Kizel	28601-24	<i>rossicus</i> left maxilla	OxA-19564	32,940 ± 190	-21.1	35,832	34,423	35,128	
UKZ-03	Kizel	28601-12a	<i>rossicus</i> left maxilla	OxA-19563	32,630 ± 180	-20.96	35,240	34,136	34,688	
-	Kizel	-	-	OxA-16960	31,870 ± 190	-21.462	34,271	33,361	33,816	From [S9]

Table S6. Radiocarbon dates for Medvezhiya and Kizel cave bears used for indirect age estimates for the sequenced samples. Related to STAR Methods.

*Calibrated using OxCal 4.2 online, based on the IntCal-13 curve.

Taxon (sample)	Reference taxon (GenBank Acc.)	Mapable reads	Mapped	Unique mapped	% Duplication	Mapped bp	Read depth*	% Covered > 2 reads
<i>praekudarensis</i> (KU1)	<i>kudarensis</i> (MH605139)	1399428212	40576	35942	11.42	1175197	69.89	97.38
brown (Ge)	<i>U. arctos</i> (EU497665)	61792045	5861	5354	8.6504	794631	47.43	96.60
brown (Uap)	<i>U. arctos</i> (EU497665)	140333181	73626	67049	8.93299	3037226	181.29	99.13
black (ERS781634)	<i>U. thibetanus</i> (NC_009971)	167698034	138701	31563	77.2439	2824722	168.19	99.23
polar (SRS412584)	<i>U. maritimus</i> (NC_003428)	31203972	32947	20507	37.7576	2001068	117.59	95.85
polar (SRS412585)	<i>U. maritimus</i> (NC_003428)	20357905	16691	13225	20.7657	1239153	72.82	95.84
<i>kanivetz</i> (B04)	<i>spelaeus</i> (EU327344)	380166888	169096	129959	23.1448	5925633	352.51	98.81
<i>rossicus</i> (B04)	<i>spelaeus</i> (EU327344)	368057543	242012	189019	21.8968	8010665	476.54	98.89
<i>eremus</i> (WK01)	<i>spelaeus</i> (EU327344)	335628787	157015	137148	12.6529	5817044	346.05	98.64
<i>kudarensis</i> (HV72)	<i>kudarensis</i> (MH605139)	252663833	133306	106436	20.1566	5894257	350.56	99.55

Table S7. Details of mitochondrial genome reconstruction. Related to STAR Methods.

*Mapped bp divided by reference genome size.

SUPPLEMENTAL REFERENCES

- S1. Barlow, A., Fortes, G.M.G., Dalen, L., Pinhasi, R., Gasparyan, B., Rabeder, G., Frischchauf, C., Paijmans, J.L.A., and Hofreiter, M. (2016). Massive influence of DNA isolation and library preparation approaches on palaeogenomic sequencing data. *BioRxiv*, 075911.
- S2. Barlow, A., Cahill, J.A., Hartmann, S., Theunert, C., Xenikoudakis, G., Fortes, G.G., Paijmans, J.L.A., Rabeder, G., Frischauf, C., Grandal-d'Anglade, A., *et al.* (2018). Partial genomic survival of cave bears in living brown bears. *Nat. Ecol. Evol.* 2, 1563–1570.
- S3. Barlow, A., Hartmann, S., Gonzalez, J., Hofreiter, M., and Paijmans, J.L.A. (2020). Consensify: A Method for Generating Pseudohaploid Genome Sequences from Palaeogenomic Datasets with Reduced Error Rates. *Genes (Basel)*. 11.
- S4. Cahill, J.A., Green, R.E., Fulton, T.L., Stiller, M., Jay, F., Ovsyanikov, N., Salamzade, R., St. John, J., Stirling, I., Slatkin, M., *et al.* (2013). Genomic evidence for island population conversion resolves conflicting theories of polar bear evolution. *PLoS Genet.* 9, e1003345.
- S5. Kumar, V., Lammers, F., Bidon, T., Pfenninger, M., Kolter, L., Nilsson, M.A., and Janke, A. (2017). The evolutionary history of bears is characterized by gene flow across species. *Sci. Rep.* 7, 1–35.
- S6. Fortes, G.G., Grandal-d'Anglade, A., Kolbe, B., Fernandes, D., Meleg, I.N., García-Vázquez, A., Pinto-Llona, A.C., Constantin, S., de Torres, T.J., Ortiz, J.E., Frischauf, C., Rabeder, G., Hofreiter, M., Barlow, A. (2016). Ancient DNA reveals differences in behaviour and sociality between brown bears and extinct cave bears. *Mol. Ecol.* 25, 4907–4918.
- S7. Lioubine, V.P. (1998). The Acheulian Epoch in the Caucasus. [In Russian] (St. Petersburg).
- S8. Pinhasi, R., Gasparian, B., Nahapetyan, S., Bar-Oz, G., Weissbrod, L., Bruch, A.A., Hovsepian, R., and Wilkinson, K. (2011). Middle Palaeolithic human occupation of the high altitude region of Hovk-1, Armenia. *Quat. Sci. Rev.* 30, 3846–3857.
- S9. Pacher, M., and Stuart, A.J. (2008). Extinction chronology and palaeobiology of the cave bear (*Ursus spelaeus*). *Boreas* 38, 189–206.